Available online at www.sciencedirect.com
ScienceDirect
Journal of Chromatography A, 1133 (2006) 149–171
JOURNAL OF CHROMATOGRAPHY A
www.elsevier.com/locate/chroma

Liquid chromatography with dual parallel mass spectrometry and ^{31}P nuclear magnetic resonance spectroscopy for analysis of sphingomyelin and dihydrosphingomyelin I. Bovine brain and chicken egg yolk

William Craig Byrdwell [a,*], Richard H. Perry [b]

[a] *USDA, ARS, BHNRC, FCL, Beltsville, MD 20904, USA*
[b] *Department of Chemistry, Purdue University, West Lafayette, IN 47907, USA*

Received 19 April 2006; received in revised form 5 August 2006; accepted 8 August 2006
Available online 30 August 2006

Abstract

Liquid chromatography coupled to atmospheric pressure chemical ionization (APCI) and electrospray ionization (ESI) mass spectrometry (MS), in parallel, was used for detection of bovine brain and chicken egg sphingolipids (SLs). APCI–MS mass spectra exhibited mostly ceramide-like fragment ions, [Cer-H_2O + H]$^+$ and [Cer-2H_2O + H]$^+$, whereas ESI–MS produced mostly intact protonated molecules, [M + H]$^+$. APCI–MS/MS and MS^3 were used to differentiate between isobaric SLs. APCI–MS/MS mass spectra exhibited long-chain base related fragments, [LCB]$^+$ and [LCB-H_2O]$^+$, that allowed the sphinganine backbone to be differentiated from the sphingenine backbone. Fragments formed from the fatty amide chain, [FA(long)]$^+$ and [FA(short)]$^+$, allowed an overall fatty acid composition to be determined. The presence of both dihydrosphingomyelin (DSM) and sphingomyelin (SM) sphingolipid classes was confirmed using ^{31}P NMR spectroscopy.

Keywords: Sphingolipids; Sphingomyelin; Dihydrosphingomyelin; APCI–MS; ESI–MS

1. Introduction

Since Hannun and Bell [1] first described the stimulus-regulated metabolism of sphingomyelin in 1989, known as the Sphingomyelin Cycle, the interest in sphingolipids (SLs) has greatly increased. SLs play two crucial roles in cellular systems: (1) they participate in cellular signaling pathways and (2) they are principal components of the structural matrices of cellular membranes (both the plasma membrane bilayer and intracellular membranes). Sphingomyelin and its metabolites have been implicated as important components of signaling cascades associated with apoptosis, cell cycle arrest, cell senescence, differentiation, T-cell receptor signaling, Ca^{2+} mobilization, lipid transport, and many more. The roles of sphingolipids in a wide variety of cell signaling pathways have been the subject of extensive review [2–11].

In their structural role, SLs have a higher gel to liquid crystalline phase transition temperature than glycerophospholipids [12–14], which means that they maintain their highly ordered state at higher temperatures (i.e. biological temperature) than glycerophospholipids [15]. SLs also have the unique characteristic that they self-associate into extended 'membrane rafts', which exhibit special characteristics, discussion of which is beyond the scope of this report, but which have been extensively reviewed [16–19]. The phase transition temperature and the degree of order of a lipid membrane is determined in great part by the composition of the fatty chains that make up the lipids [20,21]. The identities of the molecular species also have an important impact on the rate of *sphingomyelinase* turnover of SLs [14]. Thus, knowledge of the identities of the molecular species that make up a mixture of SLs is an important prerequisite for understanding their roles in cellular processes.

Phosphosphingolipids are large (∼700–900 Da) zwitterionic molecules that are not amenable to direct gas-phase analysis

* Correspondence to: Food Composition Laboratory, USDA, ARS, BHNRC, Beltsville, MD 20705, USA. Tel.: +1 301 504 9357; fax: +1 301 504 8314.
E-mail address: Byrdwell@ba.ars.usda.gov (W.C. Byrdwell).
URL: http://www.byrdwell.com.

0021-9673/$ – see front matter © 2006 Elsevier B.V. All rights reserved.
doi:10.1016/j.chroma.2006.08.014

using techniques such as gas chromatography (GC) or GC/MS. In the past, sphingomyelin species were typically derivatized to produce methyl esters from the fatty amide chain [22], while other derivatives, such as dinitrophenyl [23] or trimethylsilyl (TMS) ethers [24,25], were used for analysis of the long-chain base (LCB). TMS derivatives of ceramides, the precursors of SLs, have also been reported [26]. Bovine milk SLs have been analyzed extensively and reports on these were recently reviewed [27], while older MS applications for sphingolipid analysis were reviewed in 1993 [28]. Although effective, such methods based on derivatization are labor-intensive and time-consuming.

In 1994, Kerwin et al. [29] reported the use of electrospray ionization mass spectrometry (ESI–MS) for identification of molecular species of intact glycerophospholipids and sphingomyelin (SM) by direct infusion. Among the samples analyzed was sphingomyelin from bovine brain. The authors reported the identities of 17 sphingolipid species: 15 sphingomyelin species having varying degrees of unsaturation in the fatty amide chains, and two dihydrosphingomyelin (DSM) species (based on a sphinganine backbone) having saturated fatty amide chains.

In 1995, Han and Gross [30] used ESI–MS for analysis of bovine brain SLs by direct infusion. Six molecular species were identified as their sodiated (=natriated) adducts in positive-ion mode and as chloride adducts in negative-ion mode. All six molecular species that were qualitatively identified contained the *d*18:1 sphingenine backbone (where *d* refers to the dihydroxy long-chain base on which the sphingomyelin species was based, and the 18:1 represents the carbon chain length:degree of unsaturation of the 18:1 sphingenine long-chain base).

In 1997, Byrdwell and Borchman [31] reported the use of high-performance liquid chromatography (HPLC) coupled with atmospheric pressure chemical ionization mass spectrometry (APCI–MS) for analysis of egg yolk sphingomyelin and dihydrosphingomyelin species, and HPLC/APCI–MS and HPLC/ESI–MS analysis of human eye lens SLs. They reported six DSM molecular species, and 12 SM molecular species in egg yolk, as well as 13 DSM molecular species and 11 SM molecular species in the human lens by APCI–MS and 14 DSM molecular species and 12 SM molecular species in the human lens by ESI–MS. The human eye lens remains the only cellular system found in which DSM is the predominant SL. Percentage compositions without the use of response factors were given. They showed that separation on an amine column led to three peaks from the SLs: the first was composed of DSM species with long-chain fatty acids (FAs); the second was composed of DSM species having short-chain FAs chromatographically overlapped with SM species having long-chain FAs; and the third was composed of SM species with short-chain FAs. Within each class, fatty acids containing both saturated and unsaturated fatty acids were reported, and the longer-chain species eluted before species having shorter carbon chains.

In 1998, Byrdwell [32] reported a 'dual parallel mass spectrometer' arrangement in which two mass spectrometers, utilizing APCI and ESI, were attached to a single HPLC system to obtain both types of data simultaneously. Nineteen DSM species and 23 SM species were reported from a commercially available bovine brain sphingomyelin extract, and 15 DSM species and 19 SM species were reported from a porcine eye lens extract. Quantification was based on positive-ion spectra with no response factors applied.

Also in 1998, Karlsson et al. [33] reported the use of HPLC/APCI–MS and HPLC/ESI–MS, in separate experiments, for analysis of sphingomyelin extracts from bovine milk, bovine brain, bovine erythrocytes and chicken egg yolk. APCI–MS/MS was used to obtain structural information to identify the long-chain base and fatty acid portions of the molecules. An 'up-front' collision-induced dissociation voltage of 30 V was used. The tabulated results from bovine brain showed 15 SM species and 1 DSM species.

In 1999, Hsu and Turk used ESI–MS and MS/MS by infusion to analyze the alkali metal adducts produced with SLs [34]. Lithium, sodium and potassium adducts were examined. Lithium adducts were found to provide the most beneficial fragmentation when subjected to collisionally activated dissociation, and so these adducts were used for identification of sphingolipid molecular species. Additionally, constant neutral loss scans were performed to assist in structural elucidation. Analysis of bovine brain SLs resulted in identification of 20 sphingolipid species, all but one of which were SM species containing the sphingenine LCB. One species contained a LCB with two sites of unsaturation, and no dihydrosphingomyelin species were identified. Analysis of bovine erythrocytes resulted in identification of 26 molecular species, one of which was a saturated dihydrosphingomyelin species and eight species contained two sites of unsaturation in the LCB. Analysis of chicken egg yolk sphingolipid lithium adducts resulted in 12 sphingomyelin species.

There is some agreement, but substantial disagreement between several LC/atmospheric pressure ionization (API) MS methods (APCI–MS and ESI–MS) used for sphingolipid analysis. Byrdwell and co-workers reported substantial proportions and numerous molecular species of dihydrosphingomyelin in bovine brain and chicken egg yolk, accounting for 11.5% [32] and 8.2% [31] of SLs, respectively, by HPLC/APCI–MS. Several authors have used infusion, without prior chromatographic separation for analysis of SLs, by which approach only saturated dihydrosphingomyelin species are detected at unique masses in full scan mode. Unsaturated dihydrosphingomyelin species are isobaric with some sphingomyelin species and so cannot be readily differentiated by their protonated molecules or molecular adduct ions, although fragments in MS/MS spectra can be useful to differentiate isobaric species.

None of the studies mentioned above used ^{31}P NMR spectroscopy in combination with mass spectrometry, although Byrdwell et al. [35] did use this technique for identification of SLs in the human eye lens, the molecular species of which were later described using HPLC/API–MS [31]. The importance and value of using ^{31}P NMR spectroscopy in combination with mass spectrometry for identification of sphingomyelin and dihydrosphingomyelin in biological extracts is demonstrated herein. We hope that the present study will represent the most thorough LC/MS study done to date to describe the compositions of SLs from bovine brain and chicken egg yolk, and that it will help to clear up some ambiguity in the literature regarding SLs.

2. Experimental

2.1. Materials

All solvents were HPLC quality and were purchased from Sigma–Aldrich (Milwaukee, WI, USA) or Fisher Scientific (Fair Lawn, NJ, USA) and were used without further purification. Bovine brain sphingomyelin (BBS), chicken egg yolk sphingomyelin (CES) and dipalmitoyl phosphatidylcholine (DPPC) were purchased from Avanti Polar Lipids (Alabaster, AL, USA). All other reagents, including ethylenediaminetetraacetic acid (EDTA), ammonium formate, and glycine were purchased from Sigma–Aldrich and were used without further purification. Solutions of the commercially available SL mixtures were prepared at a concentration of 10–11 mg/mL in chloroform for qualitative analysis and percentage composition analysis. Samples used for absolute quantitative analysis by mass spectrometry had 0.5 mg/mL of DPPC added as an internal standard. For ^{31}P NMR spectroscopy experiments, a concentration of 25 mg/mL in deuterochloroform, with 10 mg/mL DPPC internal standard was prepared.

2.2. High-performance liquid chromatography

We have previously reported the separation of sphingolipids and glycerophospholipids on two amine columns in series [31,32]. However, the present study was aimed at clarifying the identities of SLs, so a different normal phase (NP) HPLC method was used that was optimized specifically for maximum resolution of the classes of sphingomyelin and dihydrosphingomyelin without regard to other phospholipid classes. The NP-HPLC system consisted of an AS3000 autosampler with a sample vial heater (set at 32 °C) and column oven (set at 57 °C), a TSP4000 quaternary gradient pump with membrane degasser, a UV6000LP diode array detection (DAD) system (Thermo Separation Products, Thermo Electron, San Jose, CA, USA) and a CH-430 column heater (Eppendorf, Westbury, NY, USA). A series of experiments (data not shown) was performed to select the optimal column temperature of 57 °C for the separation. This is similar to the temperature used by Karlsson et al. [33]. Two columns were used in series, which would not fit into the autosampler column oven, so its column oven was used only to preheat the solvent flow before entering the external column heater. Two 25 cm × 4.6 mm, 5 μm particle size, Adsorbosphere NH_2 columns (Alltech Associates, Deerfield, IL, USA) in series were used. They were joined by a piece of 0.01 in. I.D. stainless steel tubing with a circular bend such that the columns were parallel in the column heater. The columns were equilibrated at the working temperature for 1 h before the first experiment each day, and for 15 min between runs. A model MKIII evaporative light scattering detection system (Varex, Burtonsville, MD, USA) was also used as a second auxiliary detector, attached to the TSQ700 mass spectrometer. The drift tube was operated at 140 °C, with the UHP N_2 nebulizer gas at one standard liter per minute.

The solvents used were as follows: solvent A, 40% hexane (Hex)/60% isopropanol (IPA) and solvent B, 40% H_2O/60% IPA, both with 0.1% NH_4OH. The gradient program was as follows: from 0 to 50 min isocratic at 77% A: 23% B; from 50 to 55 min linear to 50% A: 50% B, held until 75 min; from 75 to 80 min recycled to initial conditions and held until 95 min to equilibrate columns. The SLs came off the column during the isocratic portion of the run, and the gradient to 50% A:50% B was used to wash off the columns. The flow rate was 0.8 mL/min throughout and 10.0 μL was injected.

2.3. Dual parallel mass spectrometry

Several types of instrument configuration were used in this work. The first consisted of an LC1/MS2 dual parallel mass spectrometer arrangement, in which positive-ion APCI–MS, MS/MS and MS^3 were performed on an LCQ Deca ion trap mass spectrometry (ITMS) system while at the same time positive-ion ESI–MS and MS/MS were performed using the TSQ700 triple-stage quadrupole instrument from the same column eluate. This arrangement was used for qualitative analysis, to identify molecular species. The APCI–MS^n data were used to assist in identification and apportionment of isobaric species. For semi-quantitative results, the LC1/MS2 arrangement was used with APCI–MS on the LCQ and ESI–MS on the TSQ, both operated in full scan mode. A third instrument arrangement used positive- and negative-ion ESI–MS, MS/MS and MS^n performed on the ion trap instrument only. Although ITMS (with either APCI or ESI) allows data-dependent scanning, in which the most abundant parent ions are automatically selected for MS^n analysis, this often leaves minor peaks unexamined. To obtain MS^n data from all molecular species, even those present at low levels, numerous runs were performed on specific subsets of parent ions manually identified from full scans, so that MS^n data were obtained from every parent ion, even those present at low levels.

The dual parallel mass spectrometers and auxiliary detectors were attached as follows: a Valco tee (Valco Instruments, Houston, TX, USA) was attached to the outlet of the second amine column. To the 90° exit of the first tee was attached a length of 0.005 in. I.D. polyetheretherketone (PEEK) tubing which went to the inlet of the diode array detector. To the outlet of the diode array detector was attached another length of 0.005 in. I.D. PEEK tubing that went to the evaporative light scattering detector. The straight-through exit of the first Valco tee was connected to a second Valco tee via a short piece of 0.010 in. I.D. stainless steel tubing. To each of the two outlets of the second tee were attached 3 ft lengths of 0.10 mm I.D. deactivated fused silica capillary tubing via an adapting ferrule. At the end of each piece of capillary tubing was connected a Valco union to a short piece of stainless steel tubing to facilitate connection to the ionization sources. Approximately 360 μL/min was split approximately equally between the two mass spectrometers.

2.4. Electrospray ionization mass spectrometry (ESI–MS) and MS^n

For dual parallel MS experiments, ESI–MS was performed on the TSQ700 mass spectrometer operating in Q3 mode, with

Q1 set to pass all ions (RF-only mode). The heated capillary temperature was 265 °C. The ESI needle voltage was 5.5 kV. The UHP N_2 sheath and auxiliary gases were operated at 35 psi and 5 mL/min, respectively. A solution of 20 mM ammonium formate in H_2O:ACN (1:4) was added directly to the ESI source as a sheath liquid at 20 μL/min, supplied from an AB 140B syringe pump (Applied Biosystems, Foster City, CA). Scans were obtained in positive-ion mode in the range *m/z* 150 to 2000 with a scan time of 1.42 s.

In early experiments, formation of dimers in the ESI source was a substantial problem. Concurrently with this study, we undertook a study to find an additive that could be used to minimize dimer formation in the ESI source. Numerous approaches were tried, ranging from organic or inorganic buffers, to EDTA or other chelating reagents such as crown ethers, to amino acids. One additive proved superior, and accomplished the almost complete elimination of unwanted dimers, while also producing minimal amounts of adducts. Dimers were most effectively suppressed using a solution of 50 mM glycine in 1 M NH_4OCOH with a pH of 8.80, added post-column via a tee supplied by a syringe pump at 50 μL/min.

For experiments in which only one mass spectrometer was used, the same source parameters given for the TSQ700 were employed for the ESI source on the LCQ Deca ion trap instrument, including the use of the ammonium formate sheath liquid. Scans were obtained on the ITMS instrument from *m/z* 200 to 2000.

2.5. Atmospheric pressure chemical ionization mass spectrometry (APCI–MS) and MS^n

In dual parallel MS experiments, APCI–MS was performed on the LCQ Deca ITMS system. The heated capillary temperature was 265 °C. The vaporizer temperature was 475 °C and the corona discharge needle current was 6.0 μA. The sheath gas flow was 40 (arb. units) and the auxiliary gas flow rate was 5 (arb. units). APCI–MS scans were obtained on the ITMS instrument in the range *m/z* 200–1200, since dimers were not observed by APCI–MS.

2.6. ^{31}P nuclear magnetic resonance (NMR) spectroscopy

Solutions of the commercially available sphingomyelin extracts in chloroform were taken to dryness in tared vials under Argon and reconstituted in deuterated chloroform with concentrations of approximately 25 mg/mL, with 10 mg/mL of dipalmitoyl phosphatidylcholine (DPPC) added as the internal standard, and to provide calibration of the chemical shift axis. The chemical shift of DPPC was set to −0.840*δ*, according to the method of Meneses and Glonek [36]. Eight hundred microliters of the sample mixture was transferred to a 5 mm NMR tube and 400 μL of the Meneses–Glonek reagent was added, prepared according to the procedure given by those authors [36]. CsOH was used for the cation to yield the Cs-EDTA complex, and H_2O was used to prepare the solution instead of D_2O, since the deuterium lock signal was provided by $CDCl_3$.

3. Results and discussion

3.1. Bovine brain sphingomyelin

Bovine brain sphingomyelin and chicken egg sphingomyelin contain smaller varieties of SL species than bovine milk, and are used to exemplify the fragments used for identification of SL molecular species. Bovine milk SLs are discussed elsewhere, and are more complex than bovine brain or chicken egg yolk, since they contain a larger diversity of long-chain bases and both odd- and even-carbon fatty amide chains. Figs. 1 and 2 show the APCI–MS total ion current chromatograms (TICs) and several extracted ion chromatograms (EICs) for bovine brain SLs containing long-chain and medium-chain fatty acids. The separation on these two amine columns gave better resolution than has been reported previously for the normal phase separation of sphingomyelin species [31–33]. Previous reports showed at most three SL peaks, whereas Fig. 1 shows additional partial chromatographic resolution into five local maxima.

Normal intact ceramide has a hydroxyl group on carbon 1 of the backbone, as well as the 3-hydroxy group and a 4,5 *trans* double bond. The structures of intact ceramide and sphingomyelin are shown in Fig. 3. During APCI–MS of SM, the 1-hydroxy group to which was attached the phosphocholine moiety leaves with the head group fragment to form a protonated phosphocholine fragment at *m/z* 184.1. A ceramide-like fragment, $[Cer\text{-}H_2O + H]^+$, is left behind, such as that shown in Fig. 4. This fragment, which represents the base peak in most mass spectra of SM obtained by APCI–MS, is equivalent to a normal protonated ceramide molecule minus a molecule of water, and is also formed by normal ceramides analyzed by APCI–MS [37]. Previously, the structures of the $[Cer\text{-}H_2O + H]^+$ fragments have been proposed to contain the three member ring structure shown in Figs. 4 and 5 [34]. Alternatively, a fragment may arise from loss of the head group to form a site of unsaturation on the remaining ceramide-like fragment. Fig. 4 shows several possible fragment structures. A table of the calculated monoisotopic masses of these fragments, as well as FA-related fragments from molecular species from 6:0 to 26:2 having 18:1 and 18:0 long-chain bases, and masses of the long-chain base fragments from 13:0 to 26:2, may be found at www.sphingomyelin.com.

3.1.1. Ion chromatograms of BBS

Ion chromatograms of saturated and monounsaturated species of dihydrosphingomyelins and sphingomyelins are shown in Figs. 1 and 2. The ion chromatogram in Fig. 1B corresponds to the saturated dihydrosphingomyelin species 24:0 DSM. Since both the fatty amide chain and the long-chain backbone are saturated, there is no sphingomyelin species that is isobaric with this DSM molecular species. The peak in Fig. 1B that elutes at 26.13 min is part of the first of the three primary sphingolipid peaks, SL1. This is a long-chain DSM species and its elution in the first sphingolipid peak is in agreement with the previous reports by Byrdwell and co-worker [31,32]. Additional MS data confirming the identities of the fatty acid chain and the long-chain base (LCB) are given below. A second peak is observed in the EIC in Fig. 1B at 29.96 min. This peak does

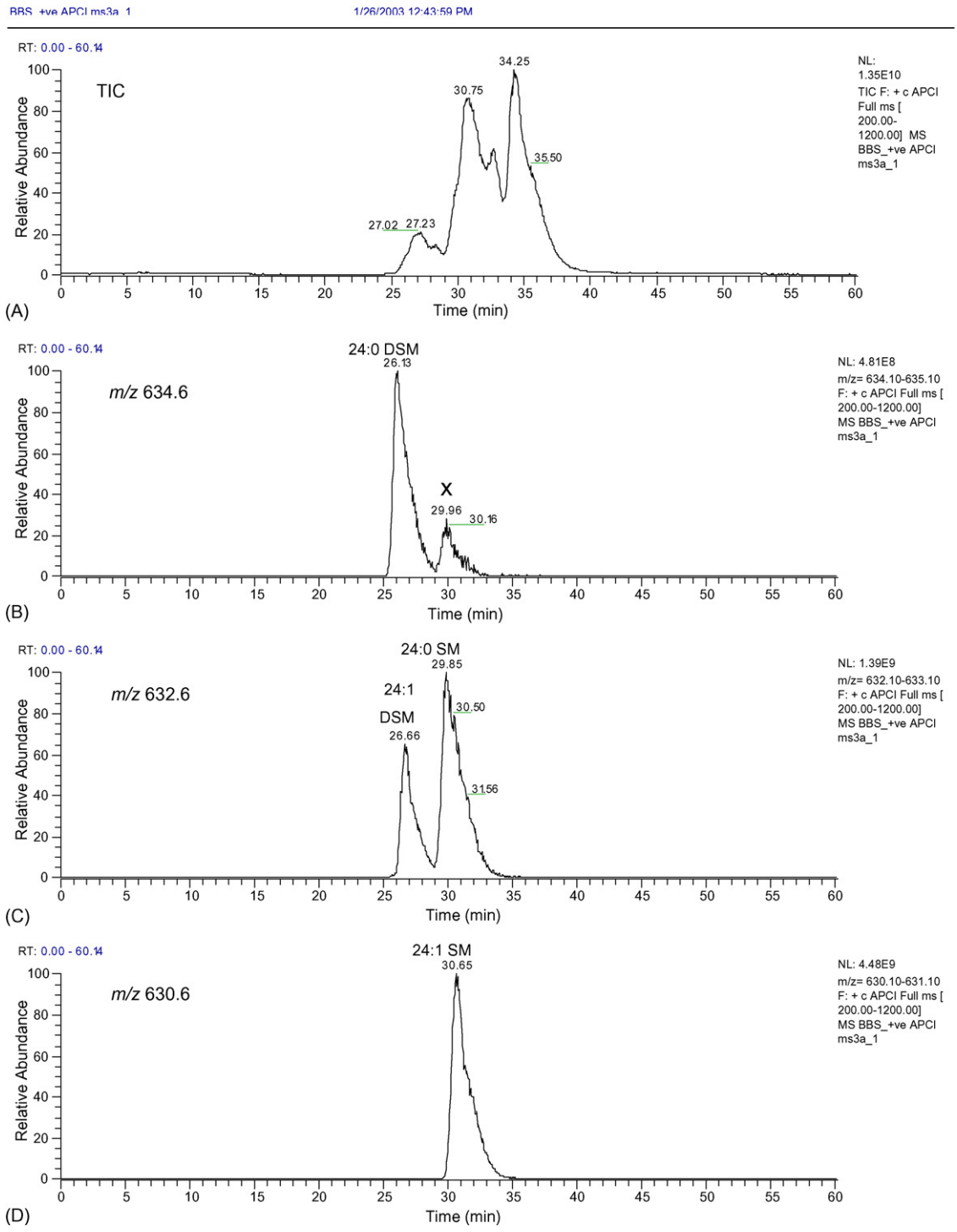

Fig. 1. (A) Total ion current chromatogram (TIC) and (B–D) extracted ion chromatograms (EIC) of long-chain DSM and SM molecular species from commercially available bovine brain sphingomyelin. Monounsaturated DSM species are isobaric with saturated SM species. $X = 2\times{}^{13}C$ isotopic contribution from 2 Th smaller species.

not correspond to a monoisotopic sphingomyelin species, but instead represents the $2\times{}^{13}C$ isotopic variant of the SM species having *m/z* 632.6. This is addressed further below, but represents an important point that must be recognized and understood to avoid misidentification of isotopic peaks. There is a corresponding substantial peak in the EIC of *m/z* 632.6, Fig. 1C, at 29.85 min. Differences in the local maxima at the top of the peaks account for slight differences in the labeled retention times for the peaks in the *m/z* 632.6 EIC, Fig. 1C, compared to the isotopic peak in the *m/z* 634.6 EIC, Fig. 1B. According to a freely available isotopic abundance calculator (Molecular Weight Calculator v. 6.22) the expected isotopic abundance of *m/z* 634.6 is 11.24% arising from the ceramide-like fragment ion at *m/z* 632.6 shown in Figs. 4 and 5. Thus, the large peak in the *m/z* 632.6 EIC

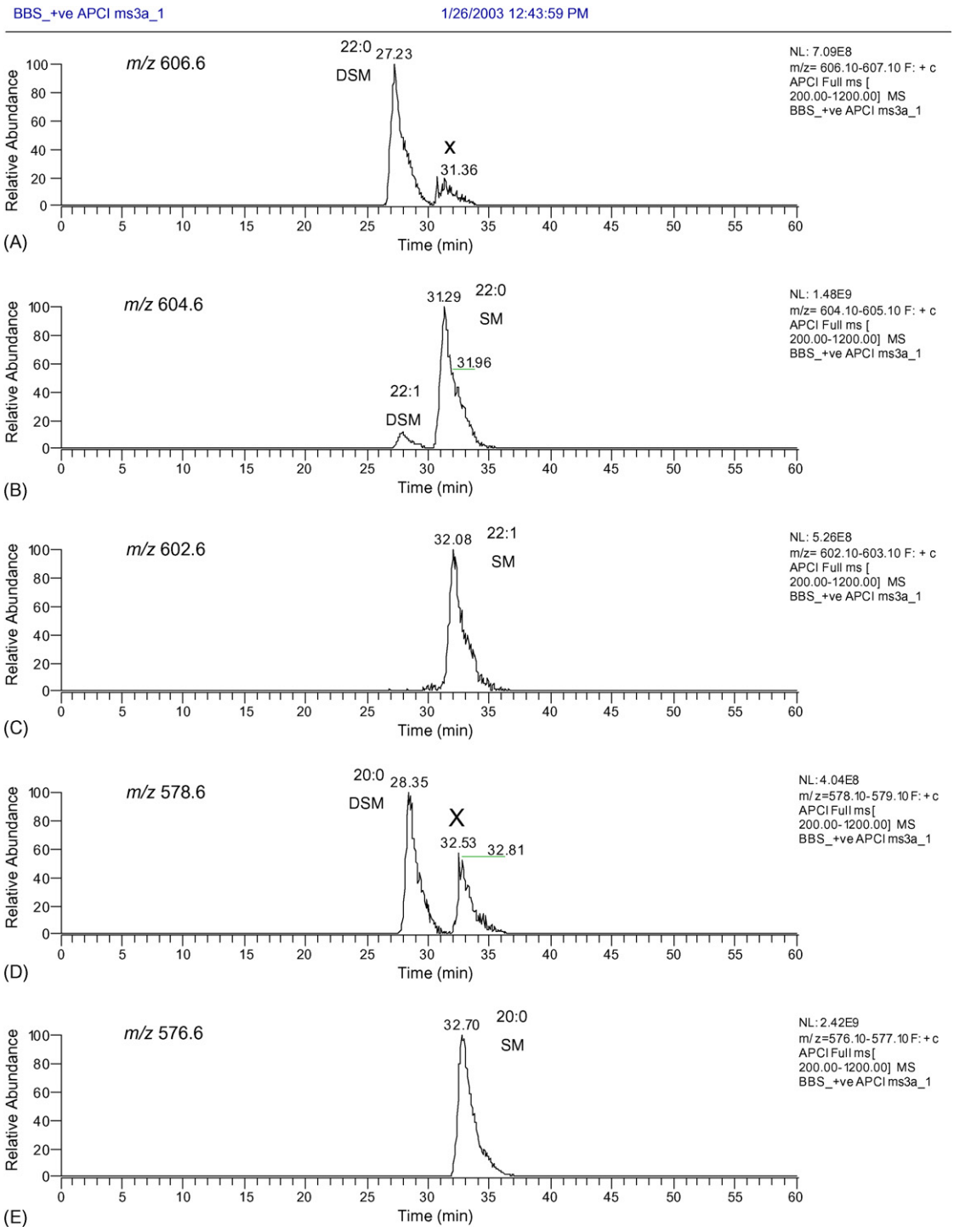

Fig. 2. Extracted ion chromatograms (EIC) of long-chain to medium-chain DSM and SM molecular species from commercially available bovine brain sphingomyelin. Monounsaturated DSM species are isobaric with saturated SM species.

should produce a peak in the *m/z* 634.6 EIC that is ~11.2% of the size of the peak in the *m/z* 632.6 EIC. A similar occurrence is in Fig. 2A in the EIC for *m/z* 606.6, which contains a peak at 31.36 min arising from the $2\times^{13}$C isotopic variant contribution from the molecular species having the monoisotopic *m/z* 604.6. Similarly, the peak in the EIC of *m/z* 632.6 at 26.66 min (Fig. 1C) contributes to the peak in the EIC of *m/z* 634.6 at 26.13 min (Fig. 1B). However, the peak at 26.13 arises mostly from an actual molecular species (24:0 DSM). The general rule can be summarized as this: if there is more of an unsaturated species (e.g. 24:1 SM) than the species having one less double bond (e.g. 24:0 SM), the $[(\text{Cer-}H_2O + H) + 2_{\text{isotope}}]^+$ contribution from the species having the smaller mass will represent a substantial contribution to the EIC of the species having the mass two units higher (we display EIC differing by 2 *m/z* because this represents a difference of one double bond). On the other hand, if the species

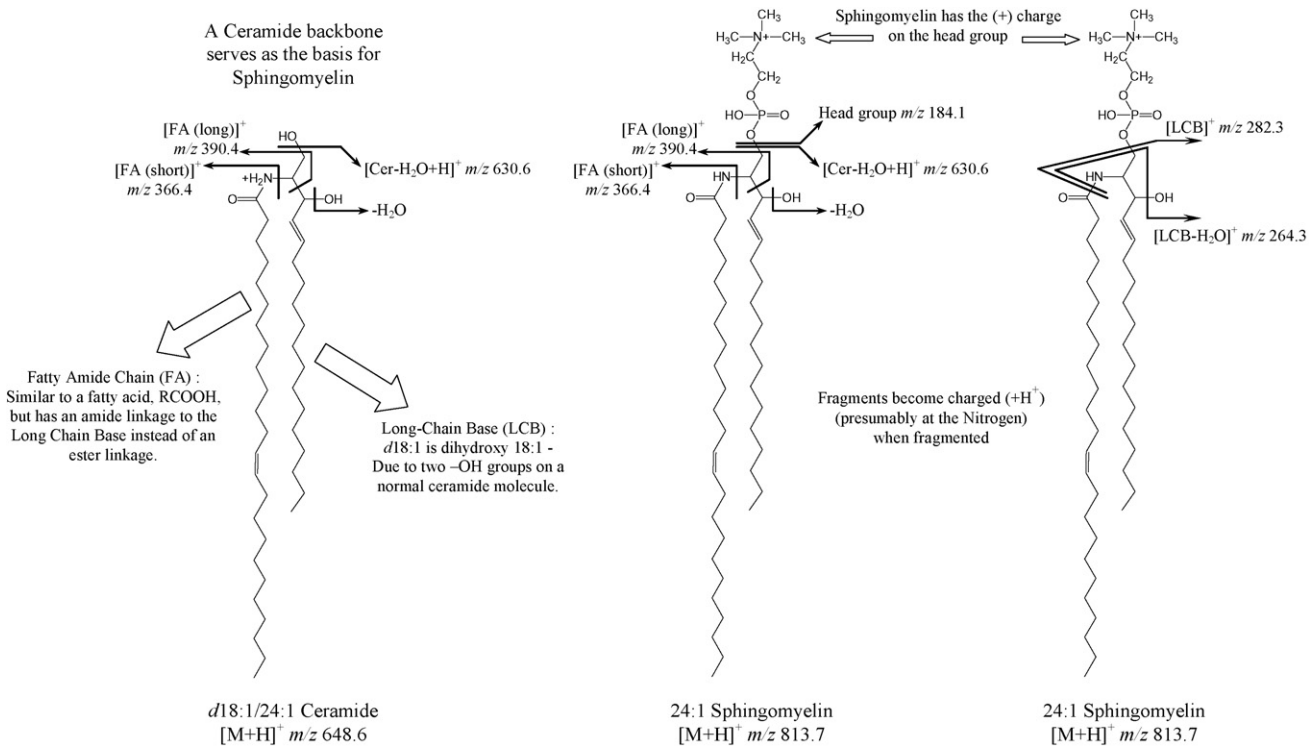

Fig. 3. Structures of ceramide and sphingomyelin.

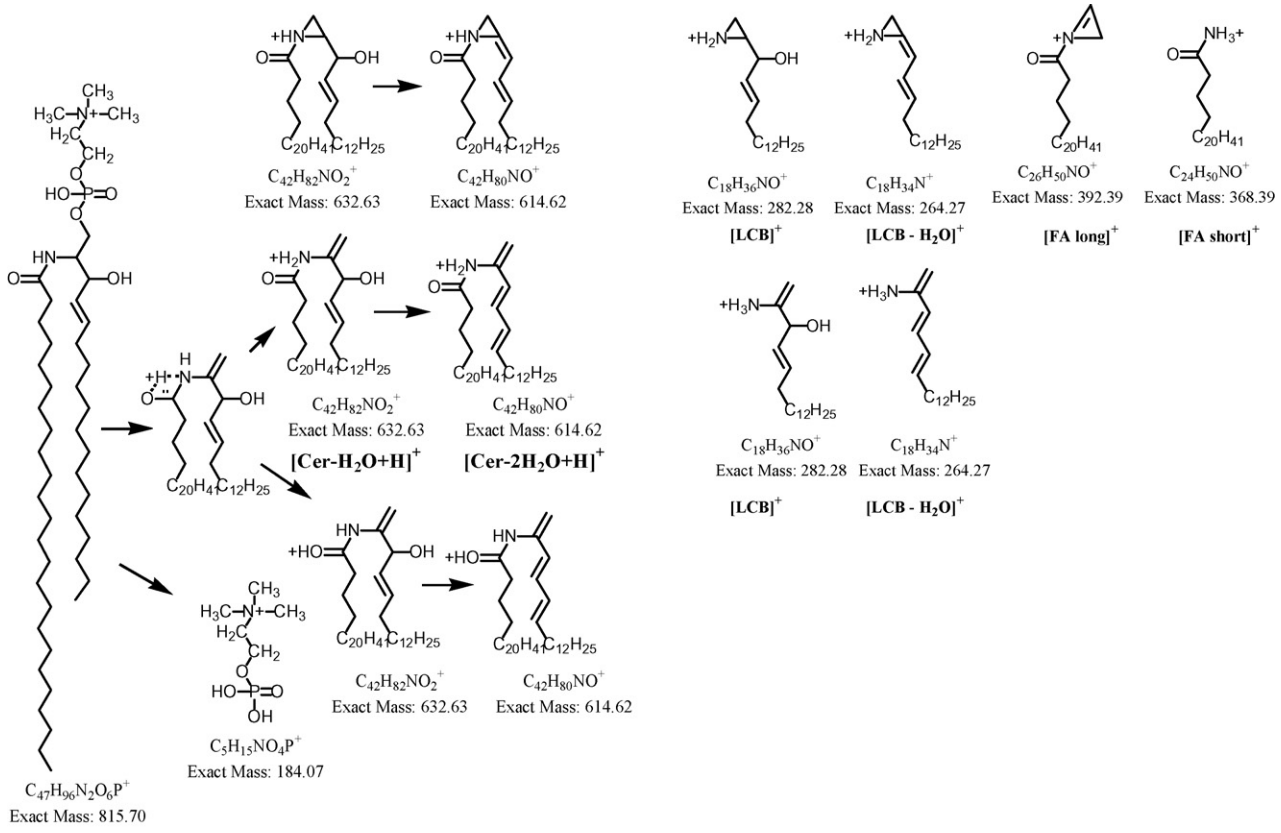

Fig. 4. Possible fragment identities for *d*18:1/24:0 (24:0 SM).

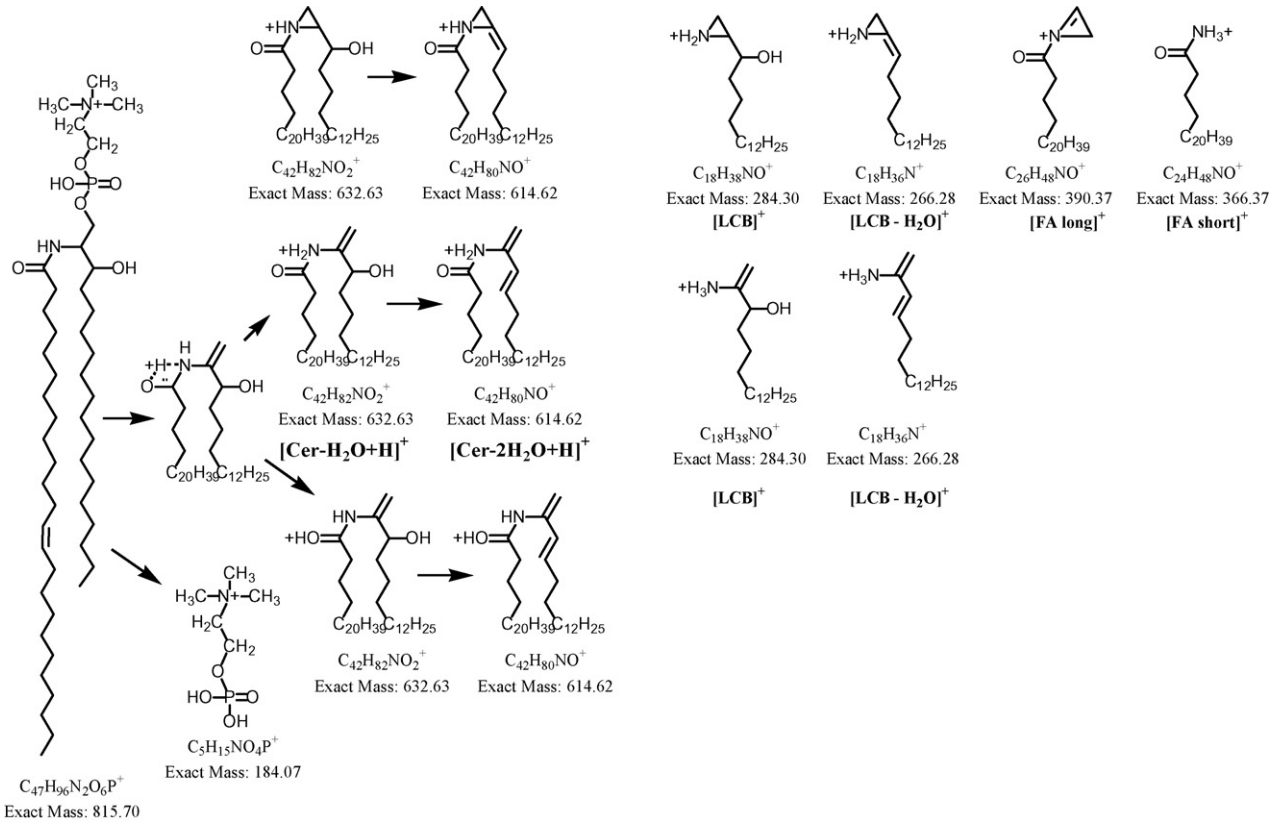

Fig. 5. Possible fragment identities for *d*18:0/24:1 (24:1 DSM).

having the larger mass is present in a larger amount (e.g. 20:0 SM), the contribution of the $[(\text{Cer-}H_2O + H) + 2_{\text{isotope}}]^+$ isotopic variant from the species with the smaller mass (e.g. 20:1 SM) will not represent a substantial contribution to the peak having the larger mass (e.g. 20:0 SM). The isotopic variant that is most often mentioned and statistically represents the highest proportion of the contribution to the $[(\text{Cer-}H_2O + H) + 2_{\text{isotopic}}]^+$ ion is the $2\times{}^{13}C$ variant, but deuterium atoms also contribute to the isotopic abundance. In fact, there is some evidence (discussed below) to suggest that there is a disproportionate likelihood that a deuterium atom can replace the labile 3-hydroxy hydrogen.

Since dihydrosphingomyelin species have often gone unreported, or only few species are reported, we present several types of data to demonstrate that they are indeed present. As Figs. 4 and 5 show, there are four primary ions that allow the long-chain base and the fatty amide chain to be identified. For SM species (Fig. 4), an ion at 282.3 represents the fragment formed by loss of the polar head group and cleavage of the amide chain between the carbonyl carbon and the nitrogen, to form an amine-containing long-chain base fragment referred to as $[\text{LCB}]^+$. This readily undergoes loss of the hydroxyl group through dehydration to form the fragment at 264.3, referred to as $[\text{LCB-}H_2O]^+$. Both of these fragments have been often reported and are used to identify the 18:1 LCB. For DSM, which lacks the 4,5 *trans* double bond, the $[\text{LCB}]^+$ fragment is at *m/z* 284.3 and the $[\text{LCB-}H_2O]^+$ fragment is at *m/z* 266.3. Two possible structures for the $[\text{LCB}]^+$ and the $[\text{LCB-}H_2O]^+$ fragments are given in Figs. 4 and 5.

There are two important fragments that are generally accepted as the basis for identification of the fatty amide chain. The first contains the intact fatty amide chain plus two carbons from the ceramide backbone, referred to as $[\text{FA(long)}]^+$. This is shown with a three-member ring in Figs. 4 and 5, although that is not the only structure that could be envisioned. The second fragment is formed by cleavage of the chain between the amide nitrogen and the LCB backbone, to give the free protonated amide, referred to as $[\text{FA(short)}]^+$.

3.1.2. Mass spectra of BBS

Fig. 6 shows the MS, MS/MS and MS^3 mass spectra averaged across the peak at 26.66 min in the EIC of *m/z* 632.6 in Fig. 1C. The full-scan spectrum, Fig. 6C, shows that *m/z* 632.7 is the base peak in the spectrum averaged from 26 to 28.5 min, indicating that it comes from the most abundant molecular species in the first chromatographic peak, SL1. The MS^2 spectrum in Fig. 6D exhibits a base peak of *m/z* 614.6, corresponding to dehydration ($-H_2O$) of the *m/z* 632.7 ceramide-like fragment shown in Fig. 5. The MS^2 spectrum shows small peaks at *m/z* 266.2 and *m/z* 284.2 that correspond to the LCB fragment from dihydrosphingomyelin, and a peak at *m/z* 390.4 that corresponds to the 24:1 fatty amide chain. The MS^3 mass spectrum of the *m/z* 614.6 fragment, Fig. 6E, contains an abundant fragment at *m/z* 266.2 that identifies the LCB as originating from dihydrosphingomyelin. The peak at *m/z* 390.3 identifies the fatty amide chain as 24:1. From these, the structure can be deduced to be 24:1 DSM. This identification is supported by the *m/z* values of the

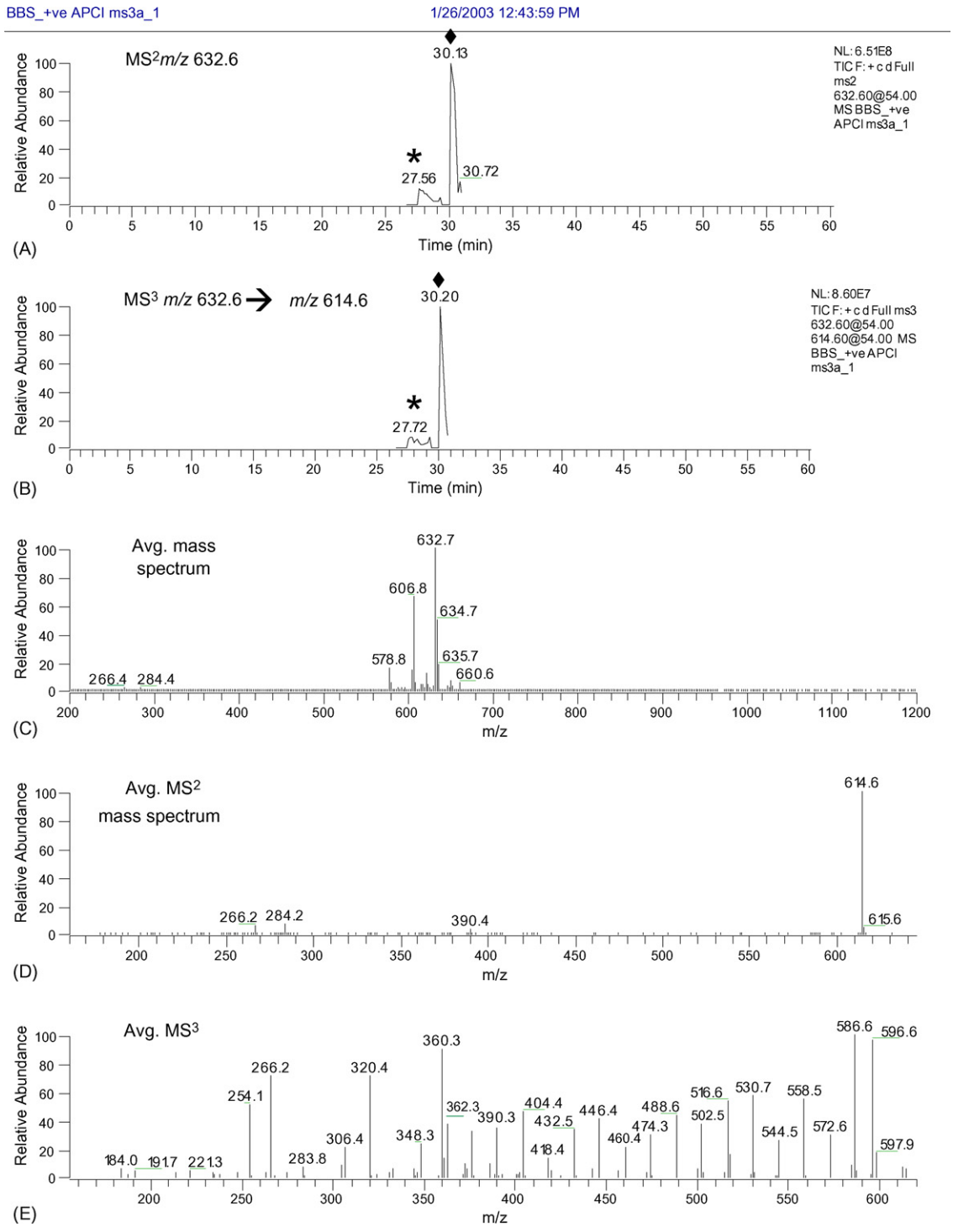

Fig. 6. (A, B) EIC of APCI–MS/MS and MS^3 scans of *m/z* 632.6, which represent the isobaric species 24:1 DSM and 24:0 SM. (C) Mass spectrum averaged from 26 to 28.5 min (see asterisks). (D) MS/MS of the *m/z* 632.7 parent, and (E) MS^3 of the *m/z* 614.6 ion. Sample was bovine brain SLs. Mass spectra of peak labeled by "♦" are shown in Fig. 7.

$[Cer\text{-}H_2O + H]^+$ and $[Cer\text{-}2H_2O + H]^+$ fragments in the full-scan MS and MS/MS scans, respectively.

Fig. 6E (compared to Fig. 7C) and figures below show that the $[Cer\text{-}2H_2O + H]^+$ fragment (base peak in Fig. 6D) from dihydrosphingomyelin underwent more extensive fragmentation in the ITMS instrument than the $[Cer\text{-}2H_2O + H]^+$ fragment from sphingomyelin (base peak in Fig. 7B). The double bond in the 4,5 position of the ceramide backbone of sphingomyelins appears to lead to a few specific fragmentation pathways for SM, whereas the lack of the double bond produces more extensive charge-remote fragmentation (CRF) and more complex MS^3 spectra for DSM. Although it is beyond the scope of this report to identify all of the fragments in the MS^3 mass spectrum of DSM, the loss of sequential methylene groups, $–CH_2–$, by CRF is indicated by

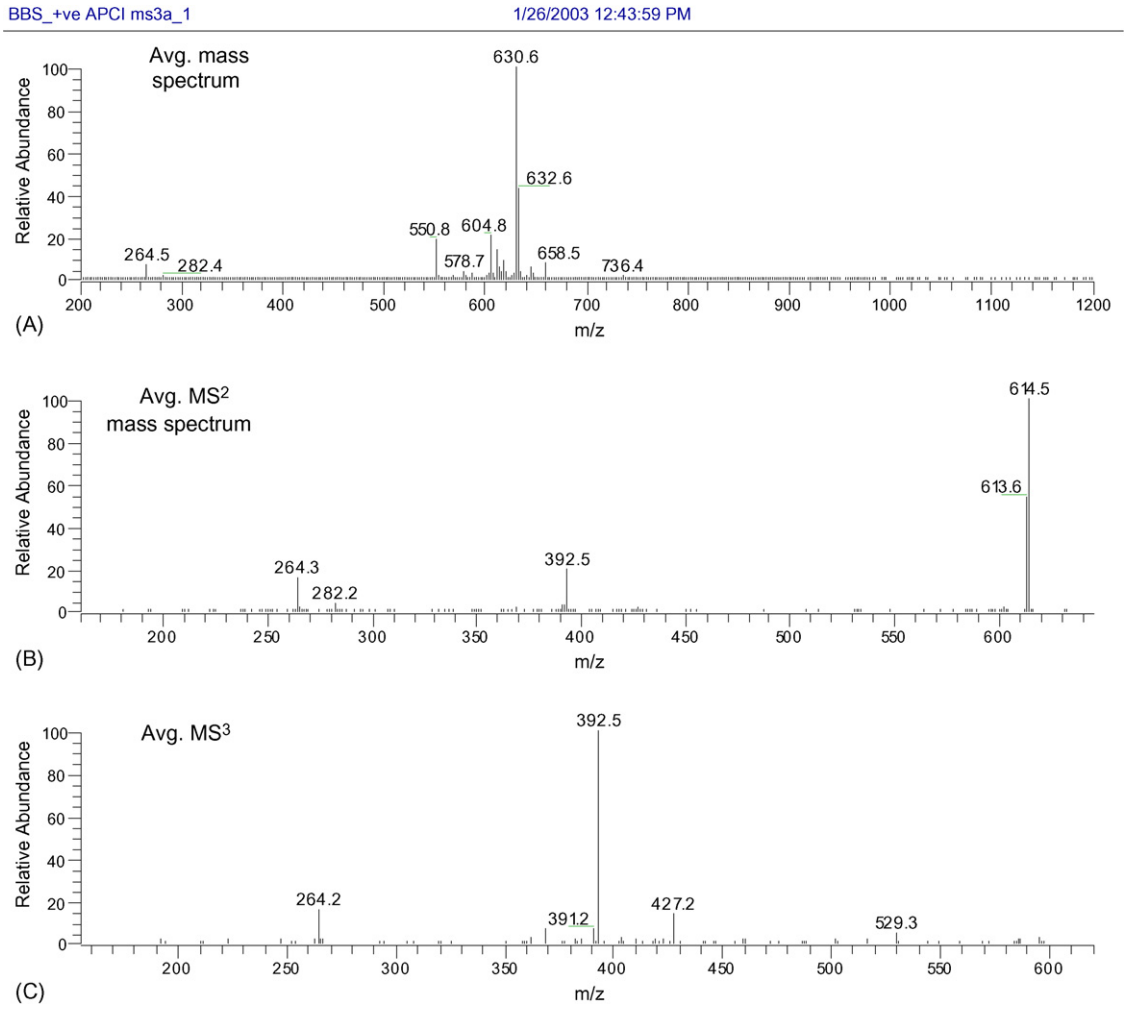

Fig. 7. (A) APCI–MS mass spectrum averaged from 29 to 32 min, shown by "♦" in Fig. 6. (B) MS/MS of the *m/z* 632.6 parent, and (C) MS^3 of the *m/z* 614.5 ion. Sample is bovine brain SLs.

the repetitive differences of *m/z* 14. The dramatic difference in the appearance of MS^3 spectra of DSM species compared to SM species serves as another piece of information to differentiate the SLs and to demonstrate the presence of DSM.

The MS/MS spectrum in Fig. 7B shows fragments at *m/z* 264.3 and 282.2 that indicate the presence of the unsaturated long-chain base, while the fragment at *m/z* 392.5 indicates the presence of the saturated 24:0 fatty amide chain, as shown in Fig. 4. The MS^3 mass spectrum in Fig. 7C contains these same ions, with the $[FA(long)]^+$ fragment being the base peak. This combination of fragments indicates the identity of the *d*18:1/24:0 SM molecular species. Of course, this also corresponds to the *m/z* 614.5 $[Cer\text{-}2H_2O + H]^+$ fragment, as well as the $[Cer\text{-}H_2O + H]^+$ fragment at *m/z* 632.6.

The *m/z* 632.6 ion is not the base peak in Fig. 7A, but it is present in an amount that was larger, but not a great deal larger, than would be expected based on calculations of the $2\times{}^{13}C$ isotope of *m/z* 630.6. The *m/z* 613.6 peak in the MS/MS spectrum of the $[Cer\text{-}2H_2O + H]^+$ fragment in Fig. 7B provides evidence of an isotopic contribution. It is well known that hydrogen atoms associated with hydroxyl groups are labile and easily substituted with deuterium atoms. If one of the isotopes contributing to the $[(Cer\text{-}H_2O + H) + 2_{isotopic}]^+$ peak at *m/z* 632.6 was a deuterium, it would be lost during dehydration and so ^2DHO would be lost (=19 Da) instead of H_2O, and would give a fragment at *m/z* 613.6 instead of *m/z* 614.5, such as that seen in Fig. 7B. In a case where there is a much smaller amount of a saturated SM molecular species than the monounsaturated species, the isotopic peak arising from the monounsaturated species could be larger than the peak arising from the monoisotopic saturated species, discussed below.

3.1.3. ^{31}P NMR spectroscopy of BBS

Since there have been so many reports that identified little or no DSM in commercially available bovine brain SM, it was necessary to employ ^{31}P NMR spectroscopy to provide a second independent method for verification of the data from mass spectrometry. Fig. 8 shows the ^{31}P NMR spectrum of the sphingomyelin that produced the mass spectra above. In 1994, Byrdwell et al. [35] identified what was at that time an unidentified phospholipid in the human eye lens. Using an amine column separation, the first of the three sphingolipid peaks was collected and subjected to ^{31}P NMR and two-dimensional correlation ^1H NMR spectroscopy (COSY). The component in the

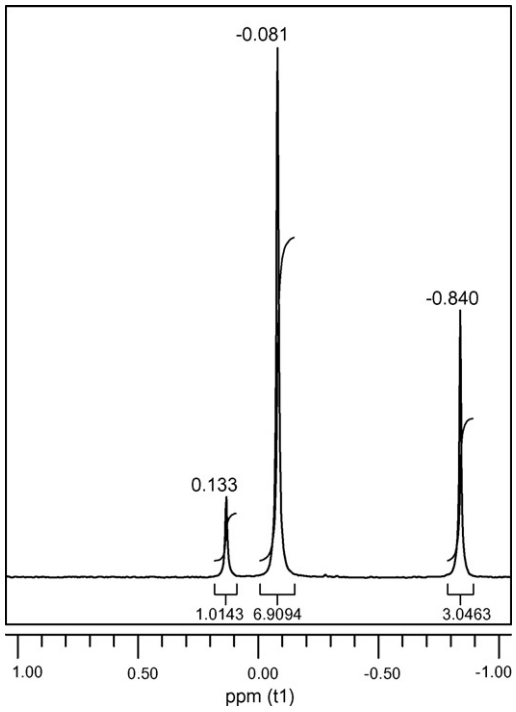

Fig. 8. ^{31}P NMR spectrum of bovine brain sphingolipids (25.1 mg/mL) with DPPC as internal standard (10.8 mg/mL) and chemical shift axis reference. DSM is at 0.133δ, SM is at −0.081δ and DPPC is at −0.840δ.

first peak showed a chemical shift at 0.13δ by ^{31}P NMR spectroscopy. The ^{1}H COSY NMR spectrum showed the absence of the 4,5 *trans* double bond, indicating a dihydrosphingomyelin backbone. The unidentified phospholipid in the human eye lens was identified as dihydrosphingomyelin. Later, Ferguson et al. [38] confirmed that dihydrosphingomyelin gives the chemical shift at 0.13δ, by analyzing DSM produced by catalytic hydrogenation of sphingomyelin. In Fig. 8, a peak at 0.13δ clearly indicates the presence of a substantial proportion of dihydrosphingomyelin in the commercially available sphingomyelin sample. Integration of the areas under the DSM peak at 0.13δ and the SM peak at −0.08δ yields a percentage composition of 12.83 ± 0.03% DSM and 87.17 ± 0.03% SM, for three replicate samples. Other reports that used mass spectrometry for analysis of bovine brain SLs which reported no dihydrosphingomyelin, or only very low levels of a few (mostly saturated) species did not employ ^{31}P NMR spectroscopy as a confirmatory technique.

Our report [32] that used HPLC in combination with ESI–MS on a TSQ 700 combined with APCI–MS on an SSQ710C instrument reported a total of 11.5% DSM with 88.5% SPC species in bovine brain sphingomyelin, without the use of response factors. Those older data and the current composition determined using ^{31}P NMR spectroscopy are in fair agreement, compared to the numerous reports that show little or no DSM present. The previous APCI–MS data from the dual parallel MS experiment were obtained using a single quadrupole mass spectrometer that did not allow the MS^n experiments that are necessary to distinguish isobaric sphingolipid species that contain different long-chain base combinations, such as *d*16:0/24:1 and *d*18:0/22:1. The data presented herein were obtained on a newer, more sensitive ion trap instrument capable of MS^n. Because of this, the presence of low levels of LCB combinations other than *d*18:0/C$_x$H$_y$ is shown here. Nevertheless, the *d*18:0/C$_x$H$_y$ DSM backbone is shown to represent approximately 97% of the BBS DSM species, while the *d*18:1/C$_x$H$_y$ SM backbone is shown to represent approximately 91% of the BBS SM species. Before presenting those data, other examples of ITMS mass spectra of DSM and SM are shown to further demonstrate the fragments used to distinguish these two classes.

Fig. 9 shows the full-scan MS, MS/MS and MS^3 mass spectra averaged across the first and second sphingolipid peaks, SL1 and SL2. Fig. 9A–C were averaged from 27 to 29.5 min, while Fig. 9D–F were averaged across the range 31–33 min. Both sets of spectra represent the *m/z* 604.7 ion, to show how these isobaric species may be differentiated. The MS/MS spectrum of *m/z* 604.7 in Fig. 9B shows fragments at *m/z* 266.3 and *m/z* 284.1, indicating a sphinganine backbone characteristic of dihydrosphingomyelin, while the fragment at *m/z* 362.3 corresponds to the FA(long) fragment identifying a 22:1 fatty amide chain. These fragments taken together indicate a *d*18:0/22:1 DSM molecular species, which is in agreement with the [Cer-2H$_2$O + H]$^+$ fragment at *m/z* 586.6, the [Cer-H$_2$O + H]$^+$ fragment at *m/z* 604.7, and elution in the first sphingolipid peak, as reported by Byrdwell and co-worker [31,32].

Fig. 9E shows the MS^2 mass spectrum of the *m/z* 604.7 peak eluted between 31 and 33 min, in SL2. The peak at *m/z* 264.3 indicates the presence of the sphingenine backbone of sphingomyelin, while the *m/z* 364.4 fragment indicates the presence of a 22:0 fatty amide chain. These fragments are observed in the MS^3 mass spectrum in Fig. 9F, as is the [FA(short)]$^+$ fragment at *m/z* 340.1, providing another indication of the presence of the 22:0 fatty amide chain. The combination of peaks identifying the sphingenine backbone and the 22:0 FA indicate that the peaks arose from the *d*18:1/22:0 SM molecular species. This is in agreement with the [Cer-2H$_2$O + H]$^+$ fragment at *m/z* 586.6, the [Cer-H$_2$O + H]$^+$ fragment at *m/z* 604.7, and elution in the second sphingolipid peak. The MS^3 spectrum of *d*18:1/22:0 SM exhibited fewer fragments than the MS^3 spectrum of the isobaric *d*18:0/22:1 DSM in Fig. 9C, similar to the difference between MS^3 spectra of *m/z* 632.6 described above. As mentioned, the presence of the 4,5 *trans* double bond influences the fragmentation pathways available for molecular decomposition, with DSM undergoing more CRF.

3.1.4. Isotopic peaks in mass spectra of BBS

The *m/z* 604.7 peak in Fig. 9D not only represents the *d*18:1/22:0 SM molecular species in SL2, but also contains any contribution from the [(Cer-H$_2$O + H) + 2$_{\text{isotopic}}$]$^+$ peak of the *d*18:1/22:1 SM molecular species that elutes in the same peak. The *d*18:1/22:0 SM species is present at ∼3.1 times greater than the amount of *d*18:1/22:1 SM (see Table 1), but fragments arising from the [(Cer-H$_2$O + H) + 2$_{\text{isotopic}}$]$^+$ peak of the *d*18:1/22:1 SM molecular species are seen. The fragment at *m/z* 585.5 in Fig. 9E appears to arise from loss of a ^{2}DHO moiety from the [(Cer-H$_2$O + H) + 2$_{\text{isotopic}}$]$^+$ fragment of *d*18:1/22:1 SM instead of loss of H$_2$O from the [Cer-H$_2$O + H]$^+$ fragment of *d*18:1/22:0 SM.

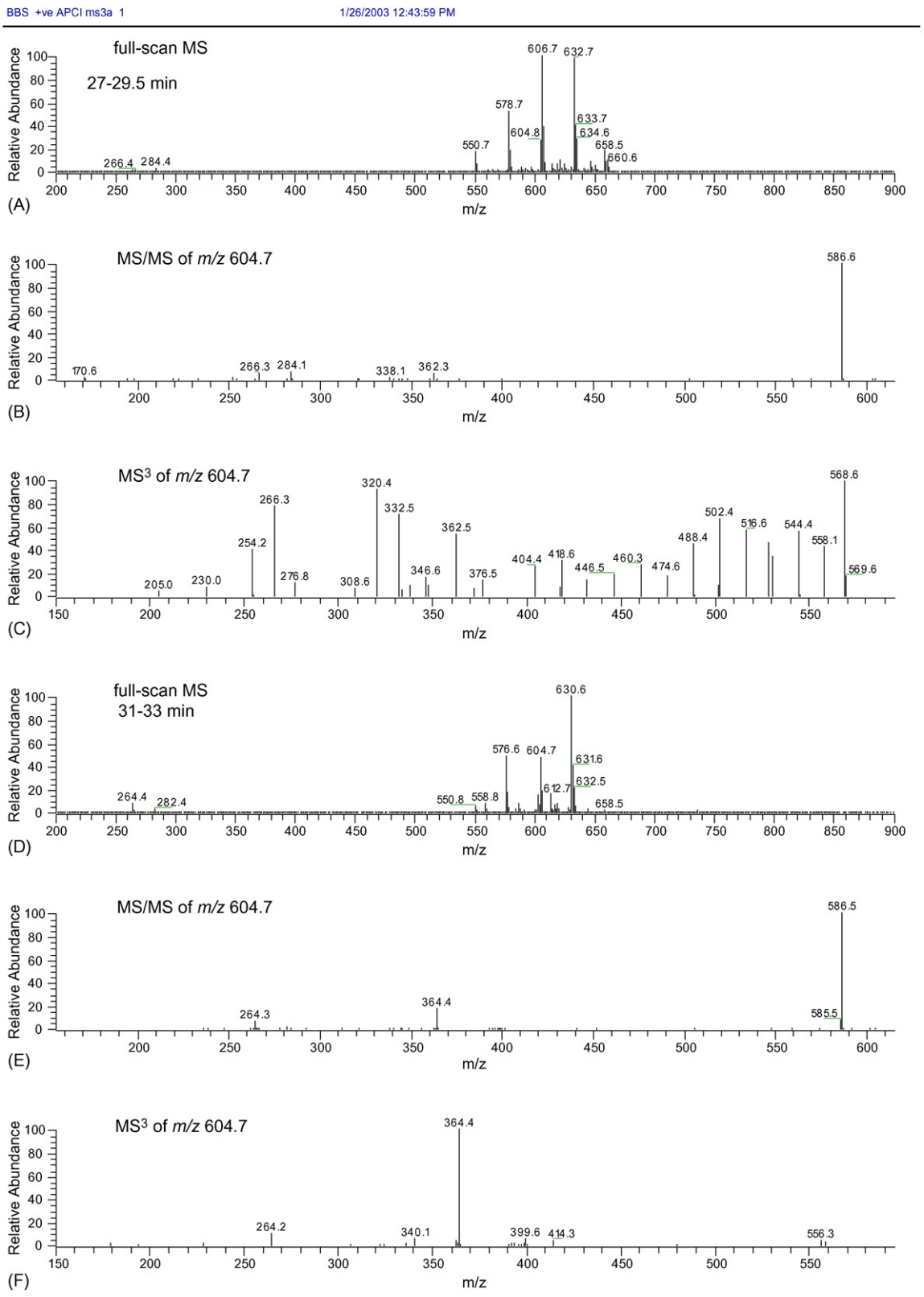

Fig. 9. Full-scan APCI–MS, MS/MS and MS^3 mass spectra of the isobaric species 22:1 DSM and 22:0 SM. MS/MS of the *m/z* 604.7 parent, and MS^3 is of the *m/z* 586.6 ion. All spectra are averaged over the time ranges indicated. Sample is bovine brain SLs.

Table 1
Semi-quantitative results for bovine brain sphingolipid molecular species based on APCI–MS

FA	DSM					SM					Net SL FA%
	16:0[a]	17:0	18:0	19:0	20:0	16:1	17:1	18:1	19:1	20:1	
	0.21[b]	1.09	97.35	0.41	0.94	0.33	0.18	91.36	1.05	7.06	
14:0								0.04		0.04	0.07[c]
15:0								0.02			0.02
16:0			0.65[d]					1.44			1.30
17:0								0.12			0.10
18:0			19.60		0.88	0.19	0.10	40.35	0.89	6.83	43.43
18:1			0.86					0.73			0.75
19:0			0.84					1.07			1.03
20:0			7.31			0.09	0.08	3.24			4.11
20:1			0.94					0.76		0.04	0.83
21:0			0.64			0.02		0.76			0.76
22:0			17.11					6.40	0.02		8.30
22:1			2.92					2.07			2.22
23:0			3.24		0.03			2.11		0.02	2.33
23:1		1.09	0.56		0.03			0.69		0.04	0.89
24:0	0.08		15.28	0.06				7.49	0.02	0.04	8.94
24:1	0.13		23.30	0.35				19.78	0.11	0.06	20.63
25:0			1.23			0.02		0.92			1.00
25:1			0.88					1.81	0.01		1.66
26:0			0.51					0.28			0.32
26:1			1.48					1.28			1.31
		DSM total = 100.00 DSM = 17.7% of SLs						SM total = 99.98 SM = 82.3% of SLs			100.00

[a] These numbers represent the identities of the long-chain bases within the SL class, given as carbon chain length: sites of unsaturation.
[b] These values represent the percentage of each long-chain base in the SL class.
[c] These values represent the net fatty amide chain composition from all molecular species in both classes of SL.
[d] These values represent the percentage of each fatty amide chain combined with each long-chain base (labeled at the top of the column) in the SL class.

This is not unexpected given the presence of a labile hydroxyl hydrogen.

The contribution from a $[(\text{Cer-}H_2O+H)+2_{\text{isotopic}}]^+$ peak can be more clearly demonstrated using the $[\text{Cer-}H_2O+H]^+$ fragment of the saturated *d*18:0/24:0 DSM species at *m/z* 634.7, which is one of the four most abundant DSM species in SL1, and has a substantial contribution from the $[(\text{Cer-}H_2O+H)+2_{\text{isotopic}}]^+$ peak of the *d*18:0/24:1 DSM species, which is the most abundant DSM molecular species. Fig. 10 shows the full-scan MS, MS/MS and MS^3 mass spectra averaged across the maximum of the *m/z* 634.7 EIC in SL1. Fig. 10A shows that the *m/z* 634.7 peak is present in an amount that is greater than expected solely from calculation of the $[(\text{Cer-}H_2O+H)+2_{\text{isotopic}}]^+$ peak of *d*18:0/24:1 at *m/z* 632.7, indicating that the *d*18:0/24:0 DSM species is also present. Fig. 10B shows a large peak at *m/z* 615.6 arising from loss of ^{2}DHO from the $[(\text{Cer-}H_2O+H)+2_{\text{isotopic}}]^+$ peak of *d*18:0/24:1, indicating that the isotopic peak represents a substantial contribution to the *m/z* 634.7 mass. Nevertheless, the peaks at *m/z* 392.4 and *m/z* 368.4 in Fig. 11B indicate the presence of the 24:0 fatty amide chain, along with *m/z* 284.2 and 266.3 that show the sphinganine LCB backbone, indicating that *d*18:0/24:0 is the major species present. The MS^3 spectrum of *m/z* 615.6 in Fig. 10C exhibits a $[(\text{LCB-}H_2O+H)+1_{\text{isotopic}}]^+$ isotopic peak at *m/z* 267.3 that arose from a normal sphinganine backbone (*m/z* 266.3) plus a ^{13}C. The *m/z* 615.6 in Fig. 10B had already lost a ^{2}DHO, so only one isotope, ^{13}C, remained in the molecule, either on the backbone fragment or the fatty amide chain. Therefore, Fig. 10C shows fragments arising from both normal and ^{13}C-containing backbone fragments and fatty amide chain fragments. Since this was a DSM species, it underwent more extensive fragmentation during MS^3 than the analogous SM species. When SLs are analyzed without prior chromatographic separation, all species of both DSM and SM and their isotopic variants would contribute to the mass spectrum. For instance, *m/z* 634.7 would represent 24:0 DSM, 24:1 DSM + 2×^{13}C, and 24:0 SM + 2×^{13}C, while *m/z* 632.7 would represent 24:1 DSM, 24:0 SM, and 24:1 SM + 2×^{13}C.

3.1.5. Semi-quantitative results for BBS

Semi-quantitative results for bovine brain SLs were obtained using dual parallel runs in which no MS^n was performed, so the peaks were not interrupted by MS/MS and MS^3 scans. Semi- quantification by APCI–MS was performed based on the sum of integrated areas under peaks in EICs corresponding to the $[\text{Cer-}H_2O+H]^+$ and $[\text{Cer-}2H_2O+H]^+$ fragments, whereas semi-quantification by ESI–MS was performed using the integrated areas under peaks in the EICs of the protonated molecules $[M+H]^+$. No response factors were applied. Isobaric species with different lengths of long-chain bases contributed to the abundances of the *m/z* values of the $[\text{Cer-}H_2O+H]^+$ and $[\text{Cer-}2H_2O+H]^+$ fragments, as well as the $[M+H]^+$ ions. For instance, *d*18:1/20:0 SM is isobaric with *d*20:1/18:0 SM, which both gave a $[\text{Cer-}H_2O+H]^+$ at *m/z* 576.6. For SLs that con-

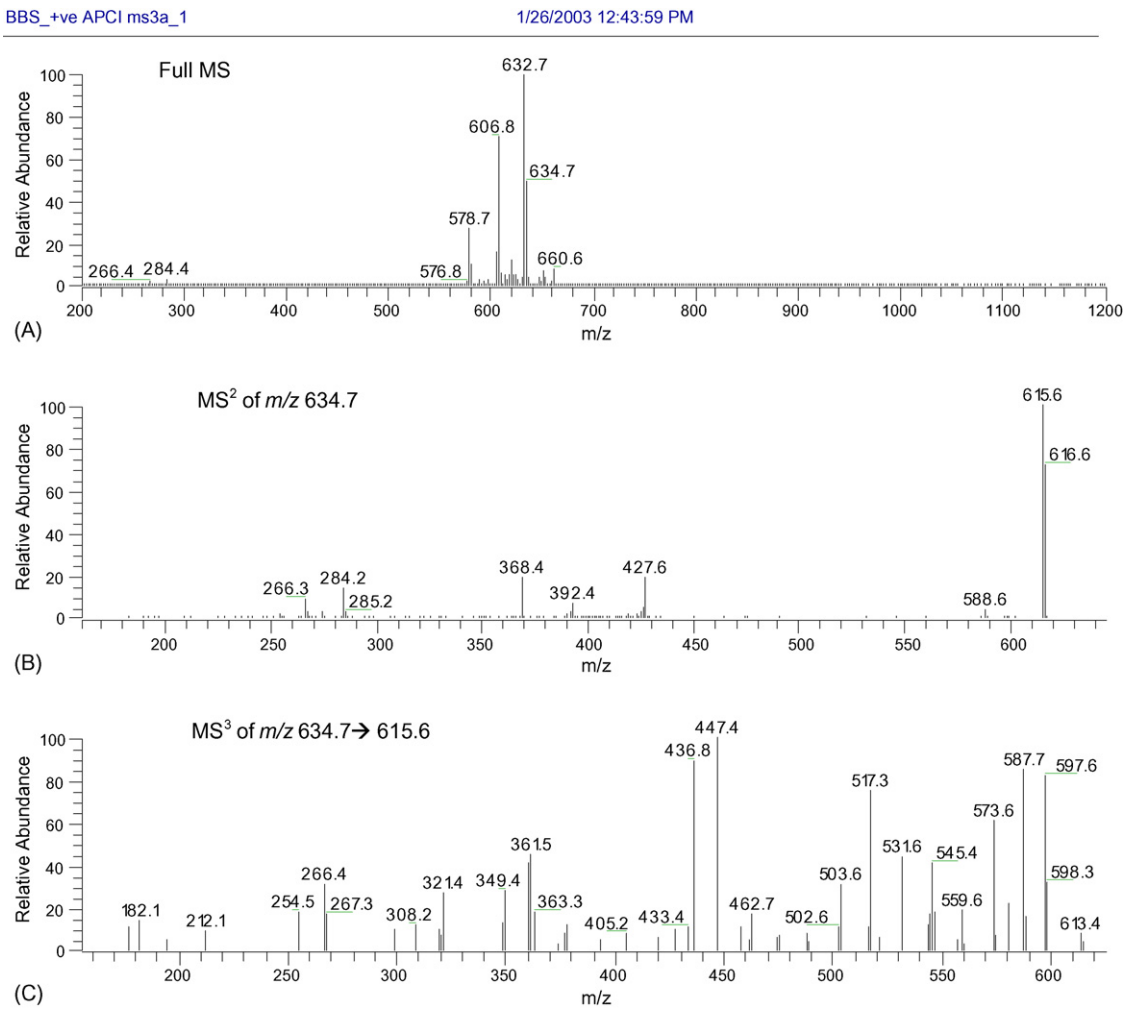

Fig. 10. (A) Full-scan APCI–MS of bovine brain SLs, (B) MS/MS of the *m/z* 634.7 precursor, and (C) MS^3 of the *m/z* 615.6 ion produced from the *m/z* 634.7 precursor.

tained any unsaturation in the molecule, whether in the FA or the LCB, the $[FA(long)]^+$ fragments in separate MS/MS runs were used to apportion the integrated areas between the isobaric species, because these were usually the next most abundant fragments in APCI–MS/MS spectra, after the $[Cer\text{-}2H_2O+H]^+$ fragment, which is not adequate to distinguish different LCB combinations. For completely saturated DSM species, the $[FA(short)]^+$ fragments were more abundant and were used to apportion the integrated areas for isobaric species. Apportionment of LCB lengths other than *d*18:1 accounted for a minority of the composition of species. In the few cases where the $[FA(long)]^+$ fragment was isobaric with the $[FA(short)]^+$ species of a coeluting molecular species, they were differentiated using the $[FA(long)]^+$ fragments in the MS^3 spectra, instead of the MS/MS spectra.

Figs. 11 and 12 represent data obtained from APCI–MS and ESI–MS, respectively, during a dual parallel mass spectrometer run used for semi-quantitative analysis. The full-scan APCI–MS mass spectra in Fig. 11 exhibit $[Cer\text{-}H_2O+H]^+$ ions (e.g. *m/z* 632.6, *m/z* 606.7 and *m/z* 578.7 in Fig. 11B) and $[Cer\text{-}2H_2O+H]^+$ ions (e.g. *m/z* 614.7 and *m/z* 588.8 in Fig. 11B), along with small abundances of protonated molecule ions. The peak at *m/z* 551.5 in Fig. 11B arose from the DPPC internal standard. All other monoisotopic peaks of ceramide-related and LCB-related fragments shown in Fig. 11 have even masses, as expected from the nitrogen rule applicable to these fragments. Fig. 12 shows the ESI–MS mass spectra across the same time windows as Fig. 11. One of the primary benefits of the dual parallel MS approach is that the molecules are eluted from a single column detected by two types of mass spectrometry simultaneously, so the retention times are virtually identical in both sets of data. The ESI–MS mass spectra in Fig. 12 exhibit almost exclusively protonated molecules. The $[M+H]^+$ for DPPC at *m/z* 734.4 is seen in Fig. 12B. The large peak at 26.06 min in Fig. 12A indicates that the ionization efficiency of DPPC by ESI–MS was greater than that of the SL species. All SL peaks in the mass spectra in Fig. 12 had odd protonated molecule *m/z* values, arising from two nitrogen atoms in the intact protonated molecules. The ESI–MS mass spectra in Fig. 12 contain an uncommon feature. Fig. 12A shows the full scan range to demonstrate that the large amount of dimers that represent a common problem in phospholipid analysis by ESI–MS (unless very dilute solutions are used) are almost completely absent. This can be accomplished by use of the glycine in ammonium formate

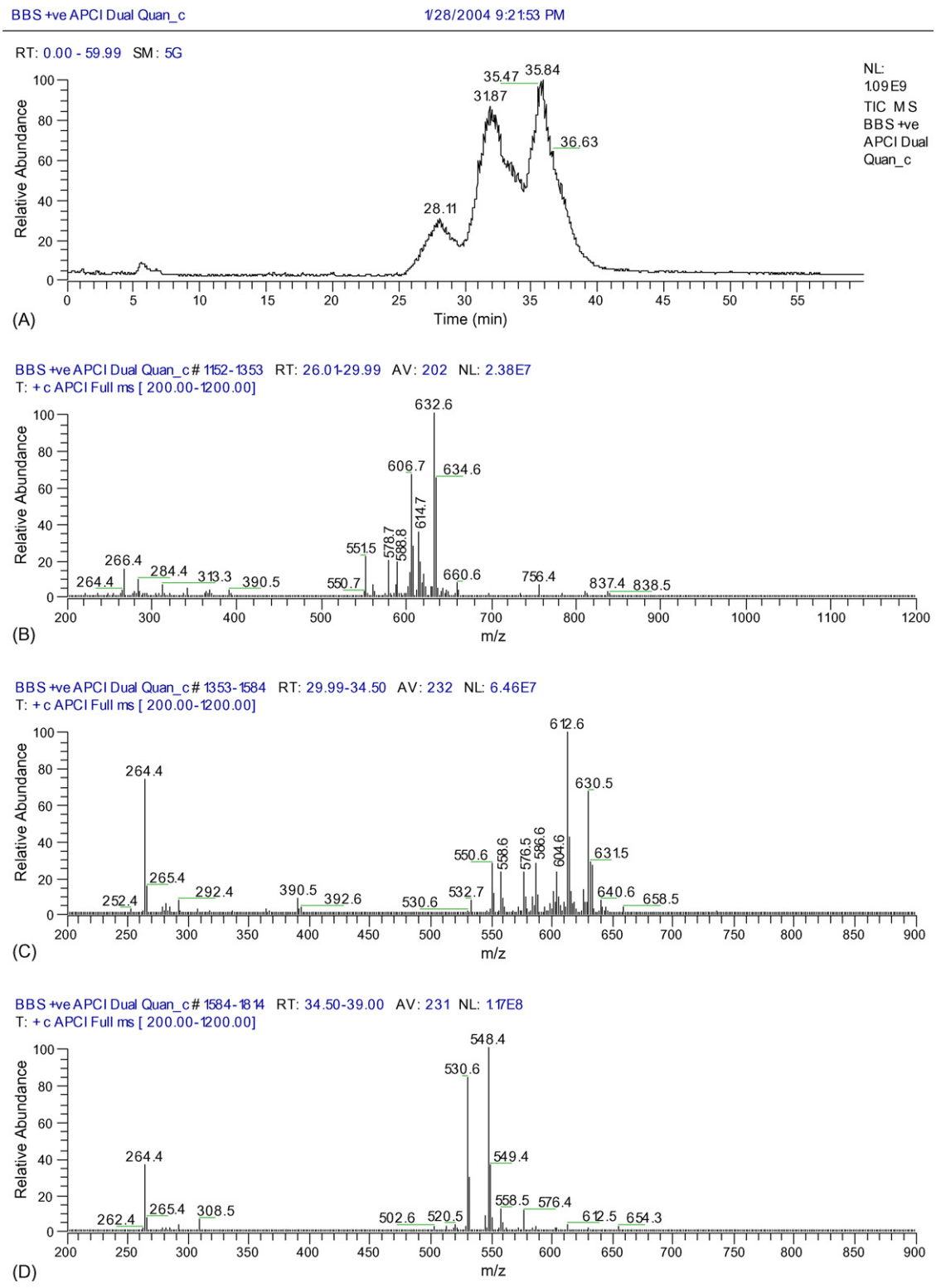

Fig. 11. APCI–MS TIC and full-scan mass spectra of bovine brain sphingolipids. (A) TIC; (B) average mass spectrum from 26 to 30 min; (C) average mass spectrum from 30 to 34.5 min; (D) average mass spectrum from 34.5 to 39 min.

solution mentioned in the materials section. Sodium adducts can be nearly completed eliminated by this same solution. Analysis of phospholipids solely as their protonated molecules facilitates qualitative analysis, and improves the quality of quantification.

Fig. 11C compared to 11B shows that sphingomyelin species produced a larger proportion of the $[LCB\text{-}H_2O]^+$ fragment (*m/z* 264.4) than dihydrosphingomyelins (*m/z* 266.4) having similar FA. Since the $[LCB\text{-}H_2O]^+$ fragment produced from DSM species is smaller than that from SM species, if this peak is

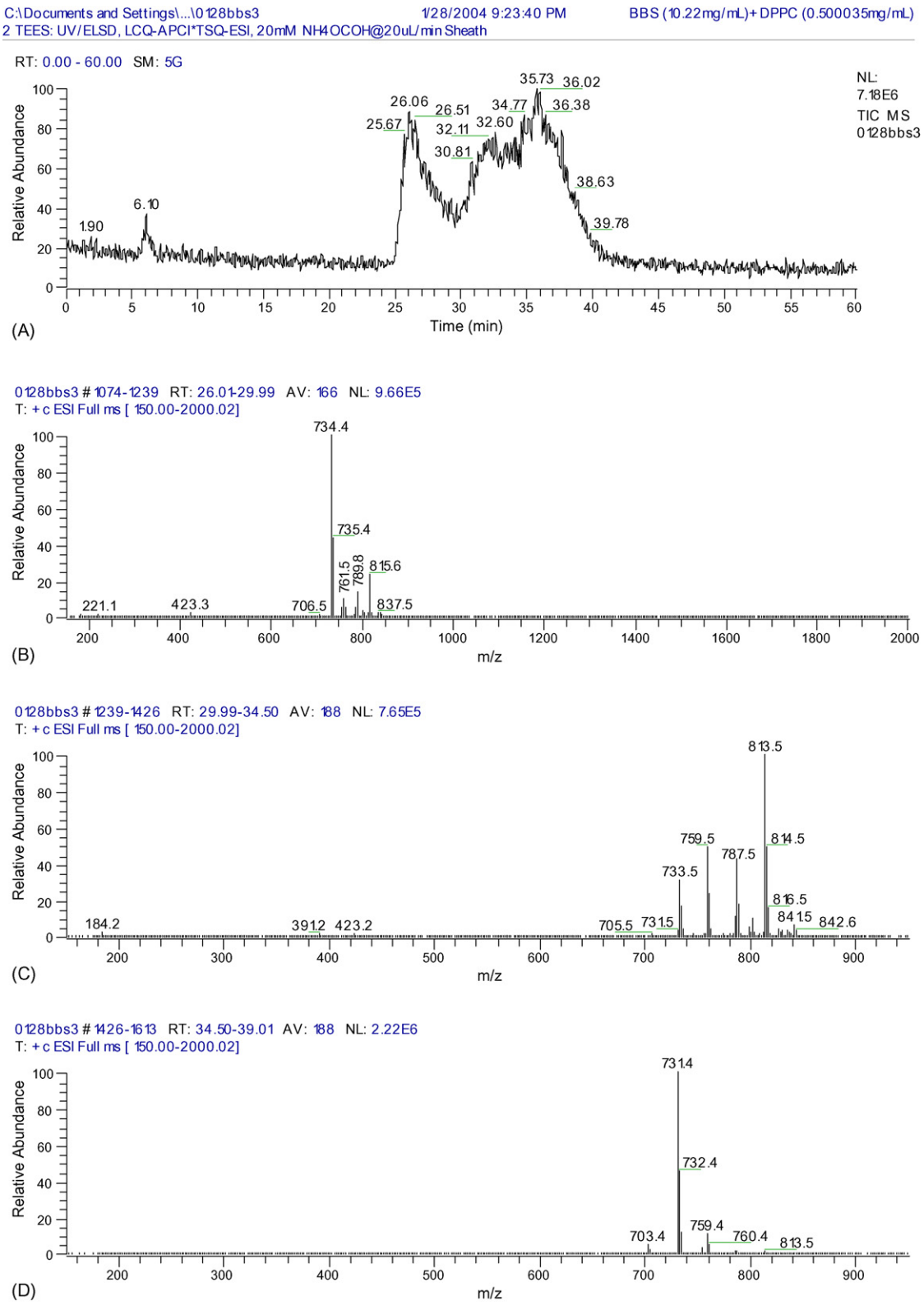

Fig. 12. ESI–MS TIC and full-scan mass spectra of bovine brain sphingolipids. (A) TIC; (B) average mass spectrum from 26 to 30 min; (C) average mass spectrum from 30 to 34.5 min; (D) average mass spectrum from 34.5 to 39 min.

used to differentiate SLs in an unseparated mixture, the DSM may be underrepresented. The DSM species may go unreported, because the small abundance of *m/z* 266.4 may not be differentiated from the abundance at *m/z* 266.4 arising from the $2\times^{13}$C variant of the large fragment *m/z* 264.4. However, when the DSM species are separated chromatographically from the SM species the *m/z* 266.4 peak is definitive for the long-chain DSM species eluted in SL1, and the $[\text{Cer-H}_2\text{O}+\text{H}]^+$ and $[\text{Cer-2H}_2\text{O}+\text{H}]^+$

fragments allow the molecular species to be identified. And when separated, the $[Cer\text{-}H_2O + H]^+$ and $[Cer\text{-}2H_2O + H]^+$ fragments from the medium- to short-chain DSM species in SL2 occur in a lower mass range than those from the long-chain SM species also eluted in SL2, allowing them to be readily differentiated and the respective molecular species identified. The medium- to short-chain SM species present in SL3 overlap with no normal DSM species, and are readily identified by their $[LCB\text{-}H_2O]^+$, $[Cer\text{-}H_2O + H]^+$ and $[Cer\text{-}2H_2O + H]^+$ fragments.

Results of the semi-quantitative analysis of the runs shown in Figs. 11 and 12 are given in Tables 1 and 2. Table 1 shows the fatty amide chains associated with each of the long-chain backbones identified by APCI–MS and MS/MS. Estimates of the compositions of individual DSM and SM species are given, along with estimates of the net fatty amide chain composition from both classes of SLs. An estimate of the percentage of each long-chain base of the two SL classes is given. Table 1 indicates that 97.4% of the DSM species were estimated to contain a *d*18:0 LCB, and 91.4% of the SM species were estimated to contain the *d*18:1 LCB. The overall composition of commercially available bovine brain sphingomyelin was 17.7% DSM species and 82.3% SM species by APCI–MS. Comparison to the ^{31}P NMR data is given below.

Table 2 shows the composition of the fatty amide chains estimated from the integrated areas under EIC of the protonated molecule ions in ESI–MS data. The goal here is not to present absolute quantitative amounts of each of the species, because standards of all SL species are not available from which calibration curves may be produced. Instead, we present the relative percentage composition and demonstrate that a wide variety of both DSM and SM species can be identified by mass spectrometry and confirmed by ^{31}P NMR spectroscopy. These data demonstrate that MS/MS and MS^3 were necessary to fully describe the combinations of long-chain bases with fatty amide chains that make up isobaric species. The most abundant species that were previously reported were confirmed in the present study. Both APCI–MS and ESI–MS gave surprisingly similar overall compositions of SLs, for an average of 17.6% DSM and 82.4% SM. These values agree fairly well with results by Ramstedt et al. [39], who performed GC–MS of the *O*-trimethylsilyl (TMS) ether derivatives of bovine brain sphingomyelin separated into classes by high-performance thin-layer chromatography (HPTLC). Those authors reported 18.5% *d*18:0 LCB (DSM) and 81.5% *d*18:1 LCB (SM) for BBS. Table 2 shows additional saturated and unsaturated long-chain bases not reported by the HPTLC technique.

$$\text{SPL Amount (mg/mL)} = \frac{\text{(Total SPL Area)}}{\text{(Int. Std. Area)}} \times \text{Int. Std. Amt. (mg/mL)} \quad (1)$$

While the estimated relative compositions agree well with previous results, the data obtained by mass spectrometry must be compared to the results by ^{31}P NMR spectroscopy and to the known amount of total SLs present in the sample to determine whether these provide accurate absolute compositions, or whether response factors are necessary. When the total areas attributable to all $[Cer\text{-}H_2O + H]^+$ and $[Cer\text{-}2H_2O + H]^+$ fragment ions obtained by APCI–MS are compared to the area of

Table 2
Semi-quantitative results for bovine brain sphingolipid molecular species based on ESI–MS

FA	DSM					SM					Net SL FA%
	16:0[a]	17:0	18:0	19:0	20:0	16:1	17:1	18:1	19:1	20:1	
	0.16	1.23	97.09	0.18	1.33	0.50	0.17	90.58	0.28	8.46	
14:0								0.11		0.07	0.15
15:0								0.04			0.04
16:0			1.16			0.01		2.71			2.44
17:0								0.17			0.14
18:0			24.55		1.31	0.36	0.15	48.31	0.22	8.25	51.78
18:1			0.36					0.39			0.39
19:0			0.59					0.26			0.32
20:0			10.90			0.11	0.02	3.92			5.25
20:1			0.56					0.15		0.04	0.25
21:0			0.45			0.01		0.31			0.34
22:0			16.79					6.02	0.01		7.92
22:1			3.29					1.82			2.07
23:0			2.87		0.02			1.47		0.01	1.73
23:1		1.23	1.07		0.01			0.84		0.01	1.11
24:0	0.08		14.28	0.03				6.35	0.01	0.04	7.81
24:1	0.08		17.77	0.15				15.51	0.04	0.04	16.01
25:0			0.58			0.02		0.47			0.51
25:1			0.38					0.59	0.01		0.56
26:0			0.54					0.30			0.34
26:1			0.94					0.84			0.85
		DSM total = 99.99 DSM = 17.5% of SLs					SM total = 100.01 SM = 82.5% of SLs				100.01

[a] See footnotes in Table 1.

the internal standard, the amount of DSM and SM can be calculated according to Eq. (1).

For the APCI–MS data, this calculation gave a concentration of 11.1 mg/mL of DSM and 51.9 mg/mL of SM for a total of 63.0 mg/mL SL. Since the sample was known to contain 10.22 mg/mL of SL, and 0.500 mg/mL of DPPC internal standard, the total areas arising from APCI–MS clearly produce an overestimate of the absolute quantities of SLs present in the sample. One primary factor is likely to be that the glycerophospholipid DPPC produced one single fragment at *m/z* 551.5 arising from the diacylglycerol-like dipalmitoyl fragment ion, whereas the SLs produced two abundant fragment ions, $[\text{Cer-}H_2O + H]^+$ and $[\text{Cer-}2H_2O + H]^+$, that were added together to yield a total integrated area. Also, PC exhibited a different ionization efficiency than the SLs, evidenced by the lack of a substantial peak at 26 min from DPPC in Fig. 11A. This situation could probably be improved by use of deuterium labeled pure sphingolipid standards for both DSM and SM.

The absolute quantities of SLs determined by ESI–MS can be calculated in a similar way. Inserting the total integrated areas for $[M + H]^+$ from DSM and SM by ESI–MS into the equation above gives a composition of 0.43 mg/mL DSM and 2.03 mg/mL SM, for a total SL composition of 2.46 mg/mL. Clearly, the response of sphingolipid species compared to DPPC is not equal. The large peak at 26.06 min in Fig. 12A, which arose primarily from the 0.500 mg/mL DPPC, illustrates that ESI–MS responded better to DPPC than to the SLs. This unequal response to the internal standard resulted in underestimation of the amounts of SLs. Response factors will be required for absolute quantification by ESI–MS. The use of deuterium labeled sphingolipid standards may allow adequate quantification of this class by ESI–MS. The response between classes is reported to be more equal when dilute solutions are analyzed [40]. However, in dilute solutions, many of the molecular species present at low levels may not be identified. Furthermore, many older instruments are not sufficiently sensitive to be used for very dilute solutions. Regardless of the current shortcomings of APCI–MS and ESI–MS for absolute quantification of the SLs, the percent relative quantification within a class is in good agreement. The results in Tables 1 and 2 are in general agreement between the two approaches used. The identities of the primary molecular species in each class are in agreement. The ionization method that is better for quantification remains to be seen. However, the first important step is to realize that substantial amounts of DSM species, as well as SM, are present.

Quantification by ^{31}P NMR spectroscopy can be examined using the internal standard equation given above. The BBS samples analyzed by ^{31}P NMR spectroscopy contained an average of 10.8 mg/mL DPPC. Three ^{31}P NMR spectra gave values of 3.73, 3.80 and 3.92 mg/mL for an average of 3.82 ± 0.10 mg/mL of DSM. These spectra gave values of 25.33,

Table 3
Semi-quantitative results for chicken egg yolk sphingolipid molecular species based on APCI–MS

FA	DSM				SM				Net SL FA%
	14:0[a]	16:0	18:0	19:0	16:1	18:1	19:1	20:1	
	0.10	1.93	97.58	0.38	0.00	99.04	0.93	0.03	
12:0						0.02			0.02
14:0			1.14			0.87			0.88
15:0			0.53			0.25			0.26
16:0		0.05	81.66	0.38		77.64	0.87		78.62
16:1			4.94			1.63			1.73
17:0			2.03			3.06			3.02
18:0	0.10	1.88	3.13			4.81	0.04		4.86
18:1			1.66			1.11			1.13
18:2						0.11			0.10
19:0						0.39		0.02	0.40
20:0			0.47			1.03	0.01		1.02
20:1						0.17			0.17
21:0						0.15			0.15
22:0			0.93			2.14	0.01		2.11
22:1						0.36			0.35
22:2						0.17			0.17
23:0			0.21			0.66			0.65
24:0			0.53			1.15	0.01		1.14
24:1			0.34			2.36			2.30
24:2						0.86			0.84
25:0						0.05			0.05
26:0						0.01			0.01
26:1						0.03			0.03
	DSM total = 99.98 DSM = 3.1% of SLs				SM total = 99.99 SM = 96.9% of SLs				100.01

[a] See footnotes in Table 1.

25.86 and 26.59 mg/mL for an average of 25.93 ± 0.63 mg/mL of SM. These gave an average of 29.74 mg/mL of total SLs. This is closer to the known average amount of 25.8 mg/mL of BBS present in the sample than the absolute quantities obtained by either APCI–MS or ESI–MS. ^{31}P NMR spectroscopy appears to represent the best alternative for quantification of the absolute amounts of SLs. ^{31}P NMR spectroscopy indicated that the SLs were composed of 12.83 ± 0.03% DSM and 87.17 ± 0.03% SM. Thus, a substantial proportion of commercially available BBS is dihydrosphingomyelin, as indicated by APCI–MS, ESI–MS and ^{31}P NMR spectroscopy.

3.2. Chicken egg yolk sphingolipids

Figs. 13 and 14 show the total ion current chromatograms and average mass spectra of chicken egg yolk SLs using the dual parallel MS approach. The first observation about these figures is that the first sphingolipid peak, SL1, is virtually completely absent. There are only very low levels of long-chain DSM molecular species in chicken egg yolk SLs. Tables 3 and 4 show the compositions of the SLs. By far the most abundant DSM species is d18:0/16:0 DSM. The composition determined by the dual parallel technique using both APCI–MS and ESI–MS agrees well with the composition reported earlier [31], although the single-quadrupole system was less sensitive and so fewer molecular species were conclusively identified. The results in Tables 3 and 4 also agree well with the report of Ramstedt et al. [39] who also reported that *d*18:1/16:0 was the primary sphingolipid, and that egg yolk SLs contained some sphinganine-based species (dihydrosphingomyelins). The amount of DSM species reported by Ramstedt et al. [39] was 7.0%, determined using derivatization to the *O*-TMS ethers, followed by GC–MS. This value is higher than the value obtained by APCI–MS, which was 3.1% in Table 3, but was nearly the same as that reported by ESI–MS, which was 6.7% in Table 4.

We obtained similar percentage compositions using the two online HPLC–MS techniques. This is in contrast to a report by LC/thermospray MS [41] in which only the *d*18:1 long-chain base was reported for chicken egg SLs, with no *d*18:0 LCB species. This is not surprising, given that the earlier report was published in 1994 and used an older, less sensitive instrument along with a less sensitive ionization method. In our data, the signal to noise ratio on the ITMS instrument is better than that on the TSQ instrument, reflecting the better sensitivity on the ITMS instrument by two orders of magnitude. Modern LC/MS instruments make possible online detection of species that previously required time-consuming derivatization to identify. Also, the online chromatographic separation of SLs into the two classes on the normal-phase amine columns greatly facilitates the identification of DSM species. This is probably why another report by ESI–MS described no *d*18:0 DSM species [34]. As mentioned above, without prior chromatographic separation, only

Table 4
Semi-quantitative results for chicken egg yolk sphingolipid molecular species based on ESI–MS

FA	DSM				SM				Net SL FA%
	14:0[a]	16:0	18:0	19:0	16:1	18:1	19:1	20:1	
	0.14	2.02	97.69	0.15	0.00	99.78	0.18	0.04	
12:0						0.05			0.04
14:0			1.58			1.36			1.38
15:0			0.67			0.32			0.35
16:0		0.07	84.65	0.15		73.45	0.11		74.31
16:1			2.86			0.40			0.56
17:0			0.78			0.41			0.43
18:0	0.14	1.95	3.79			8.06	0.03		7.95
18:1			0.92			0.56			0.58
18:2						0.17			0.16
19:0						0.18		0.03	0.20
20:0			0.48			2.20	0.01		2.10
20:1						0.17			0.16
21:0						0.20			0.18
22:0			1.15			3.81	0.02		3.65
22:1						0.54			0.50
22:2						0.29			0.27
23:0			0.09			0.90			0.85
24:0			0.50			2.14			2.04
24:1			0.22			3.39			3.18
24:2						1.07			1.00
25:0						0.07			0.07
26:0						0.01			0.01
26:1						0.03			0.03
	DSM total = 100.00 DSM = 6.7% of SLs					SM total = 99.98 SM = 93.3% of SLs			100.00

[a] See footnotes in Table 1.

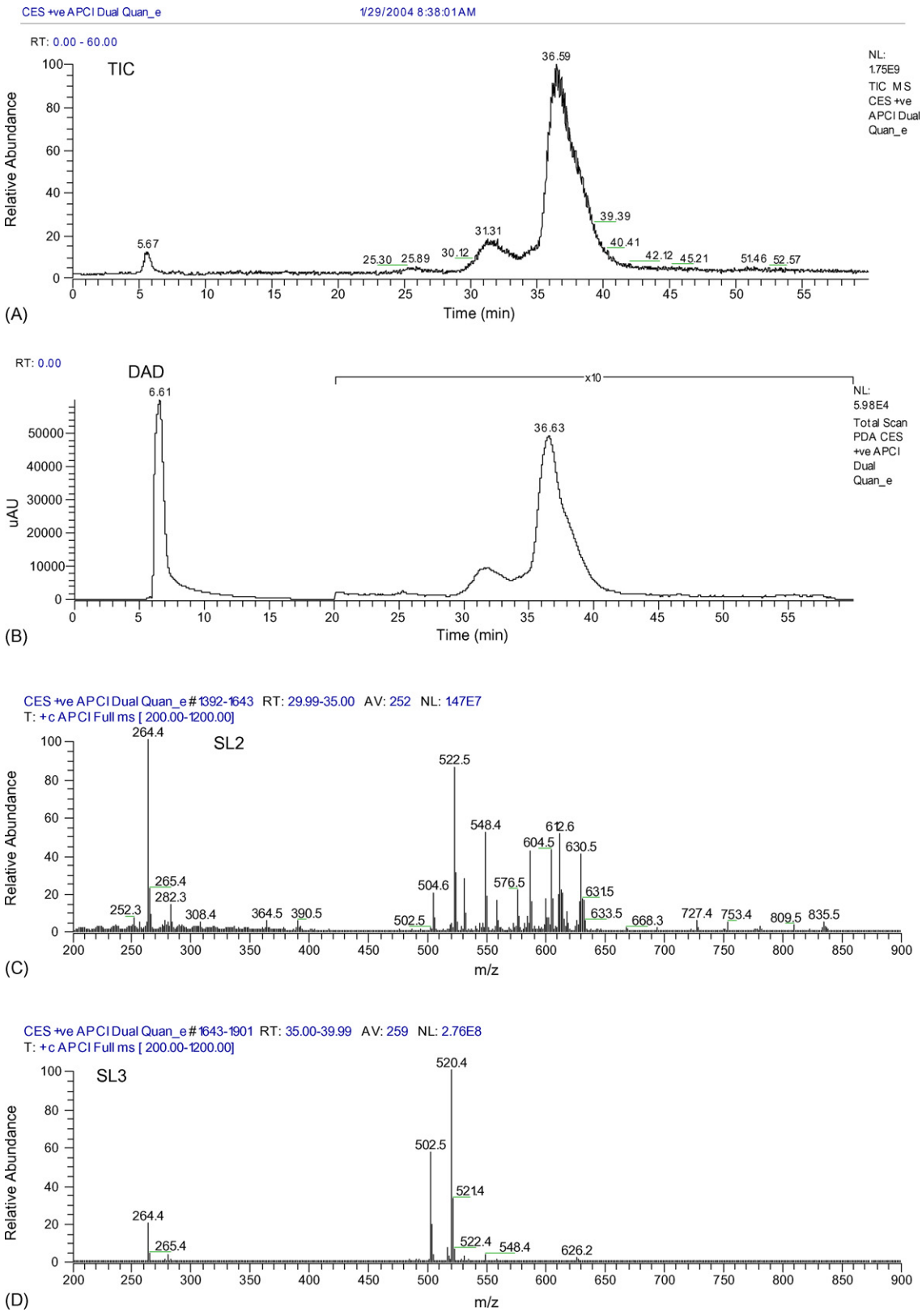

Fig. 13. APCI–MS of chicken egg yolk sphingolipids. (A) APCI–MS TIC; (B) UV DAD; (C) average mass spectrum from 30 to 35 min; (D) average mass spectrum from 35 to 40 min.

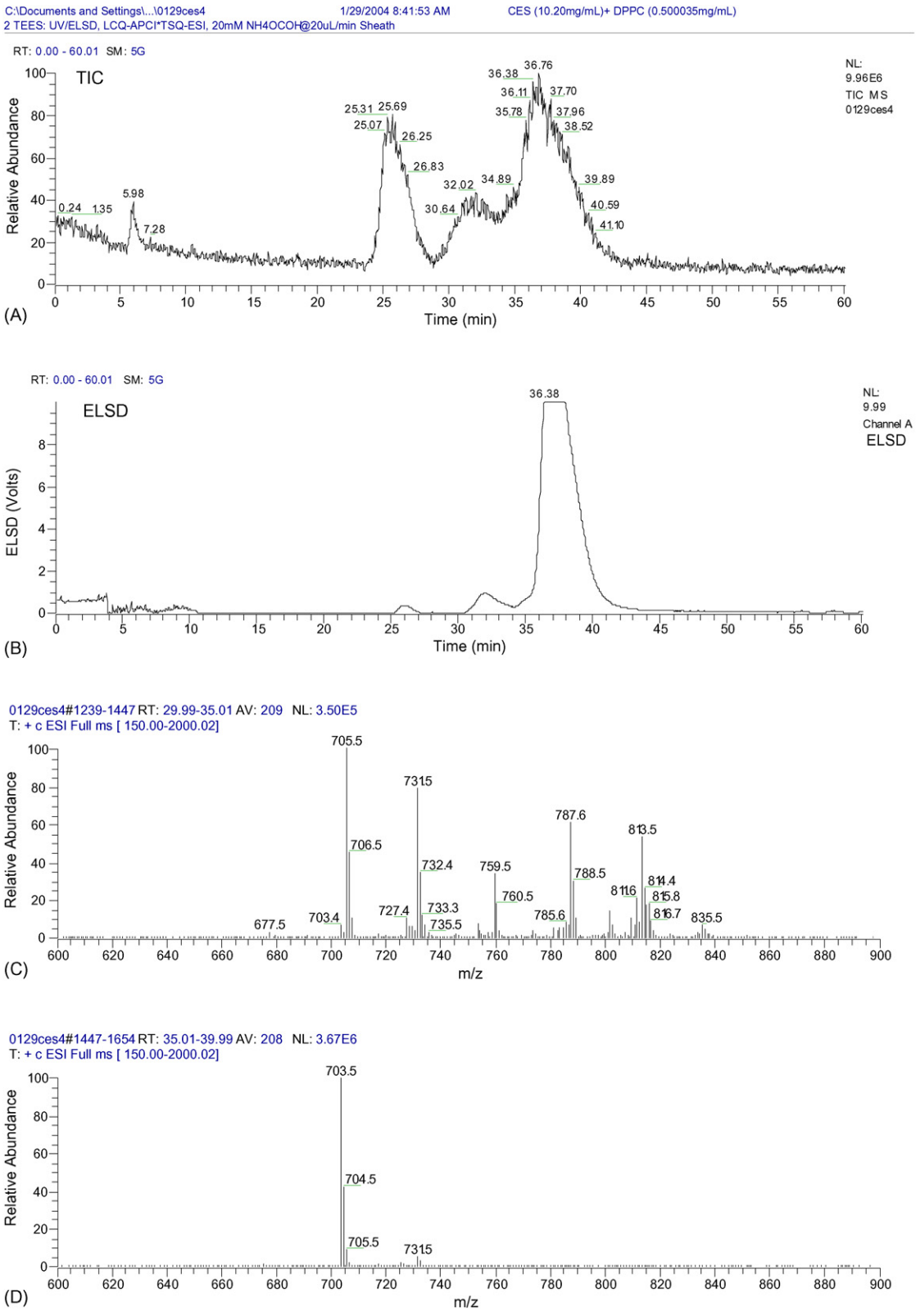

Fig. 14. ESI–MS of chicken egg yolk sphingolipids. (A) ESI–MS TIC; (B) ELSD; (C) average mass spectrum from 30 to 35 min; (D) average mass spectrum from 35 to 40 min.

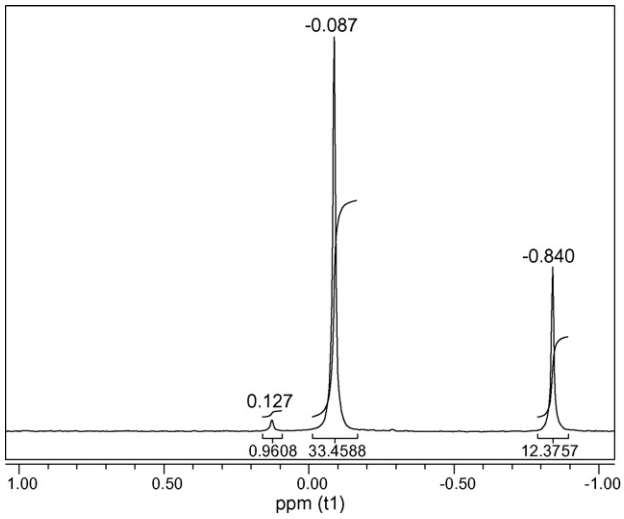

Fig. 15. ^{31}P NMR spectroscopy spectrum of egg yolk sphingolipids. DPPC internal standard is at 0.840δ. Sphingomyelin is at −0.087δ and DSM is at 0.127δ.

the DSM species with saturated FA have unique masses. DSM species that contain a monounsaturated FA are isobaric with saturated SM species, and may go unrecognized. Our results, in which online chromatographic separation was employed in combination with both ESI–MS and APCI–MS allowed more species to be identified in chicken egg yolk than any other API–MS technique reported to date. Our results provide good agreement to older time-consuming derivatization techniques that also reported noticeable amounts of DSM species.

Fig. 15 shows the ^{31}P NMR spectroscopy data for chicken egg yolk SLs. The small peak at 0.13δ gives additional evidence for the low level of DSM species in chicken egg sphingomyelin. These data indicate that chicken egg yolk contained $2.65 \pm 0.12\%$ DSM and $97.35 \pm 0.12\%$ SM, for three replicates. The data obtained by APCI–MS agrees better with the data obtained by ^{31}P NMR spectroscopy than the semi-quantitative results obtained by ESI–MS.

4. Conclusions

We have described herein the analysis of sphingolipids first by employing a normal-phase chromatographic system to separate the classes of DSM and SM, followed by detection using two complementary API–MS techniques, APCI–MS and ESI–MS, simultaneously in parallel. The APCI–MS technique produced primarily $[\text{Cer-}H_2O + H]^+$ and $[\text{Cer-}2H_2O + H]^+$ fragment ions, while the ESI–MS technique produced protonated molecules from each molecular species. The $[M + H]^+$ ions in the ESI–MS spectra allowed confirmation of the molecular weight of any species that were identified based on the $[\text{Cer-}H_2O + H]^+$ and $[\text{Cer-}2H_2O + H]^+$ fragments in APCI–MS spectra. Separate runs were performed to obtain APCI–MS/MS data. APCI–MS/MS of the $[\text{Cer-}H_2O + H]^+$ ion precursor gave long-chain base fragments, $[LCB]^+$ and $[\text{LCB-}H_2O]^+$, that allowed the class of sphingolipid to be determined as either a sphingomyelin or a dihydrosphingomyelin, and allowed the length of the LCB to be determined. APCI–MS/MS of the $[\text{Cer-}H_2O + H]^+$ ion produced fatty acid fragments, $[FA(long)]^+$ and $[FA(short)]^+$, that allowed the identity of the fatty acid to be identified in terms of the length of the FA chain and the degree of unsaturation.

^{31}P NMR spectroscopy data were also provided to further demonstrate and corroborate that substantial levels of DSM species are present in bovine brain SLs. Combined with the mass spectrometry data, the ^{31}P NMR spectroscopy data were conclusive for the presence of DSM species. Our results show more molecular species than have previously been reported by LC/MS. We have conclusively identified numerous dihydrosphingomyelin species that were not identified using other LC/MS techniques.

References

[1] Y. Hannun, R.M. Bell, Science 243 (1989) 500.
[2] Y. Hannun, J. Biol. Chem. 269 (1994) 3125.
[3] R.T. Dobrowsky, Y.A. Hannun, in: M. Liscovitch (Ed.), Signal Activated Phospholipases, R.G. Landes Company, Georgetown, TX, USA, 1994.
[4] R. Kolesnick, Mol. Chem. Neuropathol. 21 (1994) 287.
[5] L. Riboni, P. Viani, R. Bassi, A. Prinetti, G. Tettamanti, Prog. Lipid Res. 36 (1997) 153.
[6] D. Meyer zu Heringdorf, C.J. van Koppen, K.H. Jakobs, FEBS Lett. 410 (1997) 34.
[7] E.E. Prieschl, T. Baumruker, Immunol. Today 21 (2000) 555.
[8] J. Ohanian, V. Ohanian, Cell. Mol. Life Sci. 58 (2001) 2053.
[9] T. Levade, N. Auge, R.J. Veldman, O. Cuvillier, A. Negre-Salvayre, R. Salvayre, Circ. Res. 89 (2001) 957.
[10] N. Andrieu-Abadie, T. Levade, Biochim. Biphys. Acta 1585 (2002) 126.
[11] B.J. Pettus, C.E. Chalfant, Y.A. Hannun, Biochim. Biophys. Acta 1585 (2002) 114.
[12] Y. Barenholz, J. Suurkuusk, D. Mountcastle, T.E. Thompson, R.L. Biltonen, Biochemistry 15 (1976) 2441.
[13] D. Borchman, D. Tang, M.C. Yappert, Biospectroscopy 5 (1999) 151.
[14] M. Kuikka, B. Ramstedt, H. Ohvo-Rekila, J. Tuuf, J.P. Slotte, Biophys. J. 80 (2001) 2327.
[15] Y. Barenholz, T.E. Thompson, Chem. Phys. Lipids 102 (1999) 29.
[16] D.A. Brown, E. London, Ann. Rev. Cell Dev. Biol. 14 (1998) 111.
[17] A. Rietveld, K. Simons, Biochim. Biophys. Acta Rev. Biomembr. 1376 (1998) 467.
[18] K. Simons, D. Toomre, Nat. Rev. Mol. Cell Biol. 1 (2000) 31.
[19] K. Simons, W.L.C. Vaz, Ann. Rev. Biophys. Biomol. Struct. 33 (2004) 269.
[20] L.K. Bar, Y. Barenholz, T.E. Thompson, Biochemistry 36 (1997) 2507.
[21] X.M. Li, J.M. Smaby, M.M. Momsen, H.L. Brockman, R.E. Brown, Biophys. J. 78 (2000) 1921.
[22] W.R. Morrison, J.D. Hay, Biochim. Biophys. Acta 202 (1970) 460.
[23] W.R. Morrison, Biochim. Biophys. Acta 176 (1969) 537.
[24] R.C. Gaver, C.C. Sweeley, J. Am. Oil Chem. Soc. 42 (1965) 294.
[25] B. Samuelsson, K. Samuelsson, J. Lipid Res. 10 (1969) 47.
[26] B. Samuelsson, K. Samuelsson, J. Lipid Res. 10 (1969) 41.
[27] R.G. Jensen, J. Dairy Sci. 85 (2002) 295.
[28] J. Adams, Ann. Q. Mass Spectrom. Rev. 12 (1993) 51.
[29] J.L. Kerwin, A.R. Tuininga, L.H. Ericsson, J. Lipid Res. 35 (1994) 1102.
[30] X. Han, R.W. Gross, J. Am. Soc. Mass Spectrom. 6 (1995) 1202.
[31] W.C. Byrdwell, D. Borchman, Ophthal. Res. 29 (1997) 191.
[32] W.C. Byrdwell, Rapid Commun. Mass Spectrom. 12 (1998) 256.
[33] A.A. Karlsson, P. Michelson, G.J. Odham, Mass Spectrom. 33 (1998) 1192.
[34] F.F. Hsu, J. Turk, J. Am. Soc. Mass Spectrom. 11 (2000) 437.
[35] W.C. Byrdwell, D. Borchman, K.G. Porter, M.C. Yappert, Invest. Ophthal. Vis. Sci. 35 (1994) 4333.
[36] P. Meneses, T. Glonek, J. Lipid Res. 29 (1988) 679.

[37] B.J. Pettus, A. Bielawska, B.J. Kroesen, P.D.R. Moeller, Z.M. Szulc, Y.A. Hannun, M. Busman, Rapid Commun. Mass Spectrom. 17 (2003) 1202.
[38] S.R. Ferguson, D. Borchman, M.C. Yappert, Invest. Ophthal. Vis. Sci. 37 (1996) 1703.
[39] B. Ramstedt, P. Leppimaki, M. Axberg, J.P. Slotte, Eur. J. Biochem. 266 (1999) 997.
[40] X.L. Han, M.L. Gross, J. Lipid Res. 44 (2003) 1071.
[41] A. Valeur, N.U. Olsson, P. Kaufmann, S. Wada, C.G. Kroom, G. Westerdahl, G. Odham, Biol. Mass Spectrom. 23 (1994) 313.